Title: A Preliminary Analysis of Landsat Surface-Reflectance Data from Torch Lake in Antrim County, Michigan, USA from 1984 to 2023

Author: David J. Holtschlag

Email: dholtschlag@usgs.gov

Affiliation: U.S. Geological Survey, Upper Midwest Water Science Center

Peer review status:

This is a non-peer-reviewed preprint submitted to EarthArXiv.

A Preliminary Analysis of Landsat Surface-Reflectance Data from Torch Lake in Antrim County, Michigan, USA from 1984 to 2023

Oct. 04, 2024 06:31 EST (-0400 UTC)

David J. Holtschlag

Contents

Figures

Tables

Table 1. Abbreviations

Identifier	Definition
Depth	A factor variable that approximates the mean difference in reflectivity with the water-depth intervals '5-50', '50-100', '100-200', or '>200' from the reference interval of '0-5' feet.
edf	Effective degrees of freedom is a statistic for a smooth component of a GAM. The higher the edf, the greater flexibility of the corresponding smoothing spline and the greater the chance of overfitting.
EST	Eastern Standard Time (UTC minus 5 hours)
EROS	A U.S. Geological Survey Earth Resources Observation and Science Center in Sioux Falls, South Dakota.
gamma	A specification in a GAM that effects the smoothness of the estimating function. The default value of 1 was reset to 1.4 to reduce the tendency to overfit the data and making the curve less variable (wiggly).
GAM	A Generalized Additive Model is a type of regression model that contains both parametric and smooth terms. GAMs are used to attribute variations in $\ddot{\mathcal{R}}$ or $\ddot{\mathcal{R}}$ to variations in factor variables, like satellite (SAT) number (Landsat 5, 7, 8, or 9), or smooth variations in seasonal or local levels.
GBA	Golden Brown Algae, Chrysophytes chrysomonads, are a group of non-toxic aquatic organisms that are common in oligotrophic lakes, which consist primarily of diatoms along with blue-green and green algae, bacteria, and fungi.
GEE	Google Earth Engine, a catalog of satellite imagery and geospatial datasets with planetary-scale capabilities.
GIS	A Geographic Information System is a computer system that can be used to analyze and display geographically referenced information.
GTB	Grand Traverse Bay, an arm of Lake Michigan, is located along the west coast of the Lower Peninsula of Michigan. The bay is about 32 miles long and varies from 7 to 10 miles in width. The bay is further divided into an East Arm (GTBe) and a West Arm (GTBw).
Intercept	An estimated parameter in a GAM that describes the mean reflectivity given the variations in the explanatory variables.
LT05	Landsat 5 Collection 2, Level 2 surface reflectance data obtained with the Thematic Mapper sensor.
LE07	Landsat 7 Collection 2, Level 2 surface reflectance data obtained with the Enhanced Thematic Mapper sensor.
LC08	Landsat 8 Collection 2, Level 2 surface reflectance data obtained with the Thematic Mapper sensor.
LC09	Landsat 9 Collection 2, Level 2 surface reflectance data obtained with the Thematic Mapper sensor.
Local Level	In non-stationary temporal processes, the local level represents a localized estimate of the mean of a time-varying process, somewhat like a moving average. Patterns in the local level changes over time are interpreted as a local trend in this report.
N	The number of measurements or observation used in model development.
NASA	National Aeronautics and Space Administration

Identifier	Definition
NHDPlus HR	A geospatial dataset depicting the flow of water through the stream network in the United States. NHDPlus HR was built on a 1:24,000 scale or more detailed data set and the 10-meter 3D USGS Elevation Program data.
NOAA	National Oceanic and Atmospheric Administration
p-value	A statistic to describe the probability of obtaining the observed results from available data given that the null hypothesis is true. For example, the null hypothesis commonly assumes that a variable in a statistical model is insignificant. The smaller the p-value, the less likely it is that the null hypothesis is true. If the null hypothesis is rejected, the variable is maintained in the statistical model.
Path	A factor variable with two levels corresponding to satellite paths 21 and 22. Path 21 serves as the reference level, which implies a value of zero from which the parameter for Path 22 is referenced.
QA_PIXEL	A Landsat quality assurance band that provides a pixel-level indicator of the reliability of surface reflectance measurements, which can be affected by numerous factors including clouds, cloud shadows, and ice.
$\mathcal{R}$	Landsat measured surface reflectances
$\mathring{\mathcal{R}}$	$\mathcal{R}$ surface reflectances after rescaling
$\dot{\mathcal{R}}$	$\mathring{\mathcal{R}}$ rescaled reflectances after transform.
$\ddot{\mathcal{R}}$	$\dot{\mathcal{R}}$ rescaled and transformed relectances after atmospheric adjustments.
Ref.df	Reference degrees of freedom is a property of the smooth component in a GAM. The Ref.df reflects the maximum degrees of freedom possible for the form of the smooth specified.
ROI	Region of Interest delineate specific areas or subareas of lake surfaces.
SAT	A factor variable that has four levels corresponding to the series of Landsat Satellites: LT05, LE07, LC08, and LC09, which were operated sequentially with during overlapping periods from 1984 through 2023. LT05 is the reference satellite from which parameters for the remaining satellites are referenced.
SR	Surface Reflectance is a property of the reflector that can be expressed as the ratio of the amount of light reflected by a surface to the amount of light striking the surface. Surface Reflectance is commonly subdivided into the wavelength intervals (narrow bands) of light.
TSI	Tropic Status Index is a method to describe the biological productivity of a lake.
USGS	U.S. Geological Survey
UTC	Coordinated Universal Time (EST minus 5 hours)

Preliminary Analysis of Landsat Surface-Reflectance Data from Torch Lake in Antrim County, Michigan, from 1984 to 2023

By David J. Holtschlag

Abstract

This report describes an investigation of visible light reflectances from Torch Lake in Antrim County, Michigan. The oligotrophic lake is the largest inland lake in Michigan by volume and the second largest by surface area. Local residents have expressed concern that a recent, on-going proliferation of golden-brown benthic algae may be impacting the water quality and aesthetics of the lake. This report examines the seasonal and long-term variations in reflectance intensities of visible blue, green, and red light bands measured by the Landsat series of satellites from 1984 through 2023. To provide a basis for assessing possible changes, a comparable analysis was conducted for two regions having water depths greater than 100 m in Grand Traverse Bay, which lie just west of Torch Lake. Results for Torch Lake indicate that the seasonal response for the more photosynthetically active blue and green bands were similar to each other, both having a secondary peak in late August. The amplitudes of these seasonal responses were greater for water depths greater than 50 feet. In contrast, the red band for Torch Lake had a minimum in late August, which is comparable with the late August minimums in all three bands in Grand Traverse Bay. Minor seasonal differences were detected between water depths in the red band. The local levels for the blue and green bands of Torch Lake generally follow a sigmoid curve, which maintain a plateau of positive values until about 2010. After 2010, levels decline precipitously, especially in the blue band, before leveling off in 2020. Amplitudes of these trends vary more at shallower water depths. Local levels in the red band of Torch Lake and all bands of Grand Traverse Bay tend to decrease sinusodially over time. In shallow waters (<5 ft depth) where benthic areas are most readily imaged, reflectance of green, and to a lesser extent blue, light have changed relative to reflectances from deeper waters. In particular, prior to the mid-1990s, green reflectances from shallow waters were less intense than relectances from deeper waters. Following a transition period from mid-1990s to about 2014, green reflectances from shallow areas were more intense than those from deeper waters. Differences between seasonal and trend responses between bands and regions of interest may indicate differences in underlying physical, chemical, or biological processes.

Introduction

Introductory material includes background information on the circumstances and motivations for the study, purpose and scope, a description of the study area, and the attributes and limitations of available data.

Background

Since about 2014, rapid growth of the benthic golden-brown algae Chrysophyta, Chrysophyceae in Torch Lake has raised concerns about its impact on water quality and aesthetics (Torch Conservation Center 2024) and (Katz 2023). Golden Brown Algae (GBA) is comprised primarily of diatoms along with blue-green and green algae, bacteria, and fungi (Amand, Ann St. 2020), Although blooms of GBA are nontoxic to humans, the presence of GBA may affect the color and clarity of water or reflections from the lakebed in shallow areas. These changes may alter the albedo, which is a measure of the fraction of light reflected from a surface. Higher albedos of 0.75-0.90 are associated with snow and ice, while lower albedos of 0.03-0.10 associated with reflectances from (liquid) aquatic surfaces. Surface reflectance are generally positively correlated with albedo, but provide more precise, wavelength-specific information.

Global surface reflectance data has been obtained by the Landsat Program in a series of Earth-observing satellite missions (U.S. Geological Survey 2024d) jointly managed by NASA and USGS. Landsat data is processed and hosted at the USGS's Earth Resources Observation and Science (EROS) Center in Sioux Falls, South Dakota. Landsat data are composed of digital images discretized into square pixels that represent a ground surface area of approximately 30-m on as side. Pixels are grouped into scenes that form a grid that is about 106-mi by 114-mi in their north-south, and east-west dimensions, respectively. Scenes are indexed by one of 241 paths, which follow the descending orbits of the satellite. Each path is segmented into 119 rows.

Each pixel of surface reflection (SR) data contains information on multiple frequency (wavelength) intervals organized as bands with similar frequencies. Landsat 5 data has 7 bands, which included bands 1-3, corresponding to blue, green, and red frequency intervals, respectively. Landsat 7 included 8 bands by adding a panchromatic band. Data from Landsat 8 and 9 have 11 bands, which includes coastal aerosol inserted as band 1, with bands 2-4 then referencing blue, green, and red bands, respectively.

In addition to the frequency bands, Landsat data has a Quality Assessment band, *QA_PIXEL*, that provides pixel-level information on the presence of instrument, atmospheric, or surficial conditions that may affect the utility of the data (U.S. Geological Survey 2024b). In this report the *QA_PIXEL* band was used to eliminate pixels affected by the presence of clouds, cloud shadows, and ice from the analysis and computed a pixel count enumerating the number of measurable pixels in the region of interest for the scene or region of interest.

Landsat SR data in the blue, green, and red bands were used in this report to detect the color of visible light reflected from Torch Lake and parts of Grand Traverse Bay. The SR data used in this report were processed to Collection-2 Level-2 standards ($\mathcal{R}$), which provided more accurate geometric and atmospheric adjustments, and solar angle adjustments for solar zenith and azimuth angles than Collection 1 data (U.S. Geological Survey 2021). SR data in satellite missions prior to Landsat 5 seldom met these higher standards and were not included in the analysis used in the report.

SR data are unitless but indicate the intensity of incoming solar radiation that is reflected from Earth's surface to the Landsat sensor. The floating point sensor measurements are converted to 16-bit unsigned integers to facilitate data transition. Theoretically, these integers have a range of 0-65535 ($2^{16} - 1$). Scale and offset factors of 0.0000275 and -0.2, respectively, are applied to the 16-bit integers to provide a nominal range of 7,273-43,636 (U.S. Geological Survey 2024a), to span the reflection intensity interval from 0 to 1 for all surface cover types imaged by

Landsat satellites, which spans a large range of albedos. This study was restricted to surface reflection from lakes during ice-free periods, which generally have much lower reflectance properties (like albedos) than other common surface features. Thus, the usable range of Landsat SR data differed from the nominal range, especially at the higher SR values. Methods for identifying this range are discussed in a following section of this report.

At high sun elevations, (Katsaros et al. 1985) indicates that albedo (SR) is expected to be lower than at lower sun elevations, and that albedo may be higher in windy conditions due to re-suspension of bed sediment in shallow areas. Also, at high sun elevations, winds may increase the effective albedo due to greater solar reflection from areas between wave troughs and crests that form low incident angles with the sun, which are associated with sun glints during periods when white caps form. For for high sun elevations, however, the albedo for cloudy skies will be greater than the albedo for clear skies, perhaps from reflections back to the water surface from the undersides of clouds.

Despite the enhancements developed for land-specific applications, researchers caution the use of SR products for long-term water-quality studies (Rocchio, Laura E.P. 2023). The authors "found that Surface Reflectance products for Landsats 5 and 7 lack the precision to be used in rigorous water-quality studies–overestimating water body reflectance by more than 25 percent. The overestimation means that false downward trends will be found when using Landsat 5 and 7 SR time-series data in combination with that from Landsats 8 and 9."

In addition, a letter in Limnology and Oceanography (Maciel et al. 2023) cautions that the SR from land surfaces would likely have different atmospheric corrections than those targeted specifically to aquatic reflectance. Both USGS and NASA continue algorithm development and testing to provide a consistent and credible Landsat record for water-column relevant studies, and plan to support new atmospheric correction research for Collection 3 Landsat Next data (Rocchio, Laura E.P. 2023) when it becomes available.

Meanwhile, Landsat data users are advised to use the provisional Aquatic Reflectance product (U.S. Geological Survey 2024c) available from Landsat satellites beginning in 2013. Users of Landsat data also advised not to use the SR products to conduct long-term water-column trend analysis with satellite data prior to Landsat 8, unless they use band ratios or other methods to adjust for observed biases.

In response to these cautions, this report uses Landsat imagery from Grand Traverse Bay as a reference for interpreting seasonal and trend characteristics determined for Torch Lake. In addition, a method for atmospheric corrections was developed and applied to reduce bias thought to be associated with cloud cover. And finally, a factor variable was used to harmonize data from Landsat 5, 7, 8, and 9 satellites to avoid interpreting differences in sensitivities of satellite sensors and prescribed band widths as a downward trend in surface reflectances. These adaptations were needed to utilize data that spanned the time period from 1984 to 2023, when possible changes in surface reflectances were being investigated. The preliminary nature of this report as indicated in the title is intended to acknowledge the possible limitations of interpreting surface reflectance data from aquatic surfaces.

Purpose and Scope

The purpose of this study is to better understand intensity magnitudes and changes in the surface reflectances of the blue, green, and red bands of visible light from Torch Lake using data for 1984 through 2023 obtained from Landsat satellites 5, 7, 8, and 9. Adjustments to mitigate possible atmospheric effects on surface reflectance measurements were estimated and applied. Statistical models were developed to identify associations between surface reflectances and harmonize data from individual satellites, depth of water, and other selected factors to clarify seasonality and trend characteristics of surface reflectance data. A similar analysis was completed for selected regions of interest in Grand Traverse Bay to provide a basis for comparison and possible adjustment. It is

beyond the scope of this report to identify specific water-quality properties that may be changing because of the lack of systematic, comprehensive water-quality monitoring during the extensive period of analysis. In combination with other measurements and modeling efforts, however, any identified patterns in reflectance may provide a context for identifying and interpreting other changing properties. The blue, green, and red frequency bands of visible light are thought to be preferred indicator of any changes in the aesthetic appearance of Torch Lake.

Study Area

Torch Lake is in Antrim County, Michigan, and is part of a Chain of Lakes that extends about 55 miles from Beals Lake in eastern Antrim County to the East Arm of Grand Traverse Bay (fig. 1). The East and West Arms of Grand Traverse Bay lie just west of Torch Lake. The surface area of Torch Lake is 29.3 mi^2, and it has a maximum depth of about 300 ft. Tributary flow into Torch Lake from the upstream Chain of Lakes is through Clam River, a 0.22 mi connecting channel that forms the outlet of Clam Lake.

Inflow to Torch Lake is monitored at USGS streamgage 04127568 Clam Lake Outlet to Torch Lake near Alden, MI, which is located at north latitude $44^\circ 56' 33.01''$ and west longitude $85^\circ 17' 0.96''$. The drainage area at streamgage 041275685 is 198.8 mi^2. Provisional flow records from June 1, 2023, to May 31, 2024, indicate an average flow of about 321 ft^3/s.

Outflow from Torch Lake is monitored at 04127570 Torch River at County Road 593 at Torch River, MI, which is located at north latitude $44^\circ 51' 1.44'''$ and west longitude $85^\circ 19' 39.98''$. The drainage area at this gage is 275.3 mi^2. Provisional flow records from June 1, 2023 to May 31, 2024, indicate an average flow of about flow at 04127570 is about 340 ft^3/s.

Flows at both streamgages are computed on the basis of an index velocity rating (Levesque and Oberg 2012). The difference between the provisional flows from Clam Lake Outlet and Torch River are attributed to flow from unmonitored parts of the basin, differences between direct precipitation and evaporation from the surface of Torch Lake, and possible changes in the volume of water stored in Torch lakes within the period.

Based on data measured and compiled by Comprehensive Water Quality Monitoring Program (CWQMP) (Tip of the Mitt Watershed Council 1987a) and the associated Volunteer Lake Monitoring Program (Tip of the Mitt Watershed Council 1987b), Torch Lake can be classified as being in an oligotrophic state. A southern sampling site monitored on Torch Lake, located at $44.9576^o\ N,\ 85.3111^o\ W$, provided 164 Secchi disk depth (SDD) measurements from June 1991 to August 2023. The mean depth of these measurements was 22.7 ft, which generally varied seasonally from 11-38 ft. A northern sampling site at $45.0656^o\ N,\ 85.3349^o\ W$ had an average SSD of 25.2 ft based on 132 measurements from June 1993 to September 2023. The trophic status index (TSI) based on these SDDs, computed using the formula $TSI_{SDD} = 60 - 14.41 \cdot ln(SDD_{meters})$, equaled 32.1 and 30.6, respectively. Water bodies with TSI values less than 40 are considered oligotrophic, with low productivity. TSI values computed from total phosphorus and chlorophyll-A values available from CWQMP are consistent with those based on SDDs.

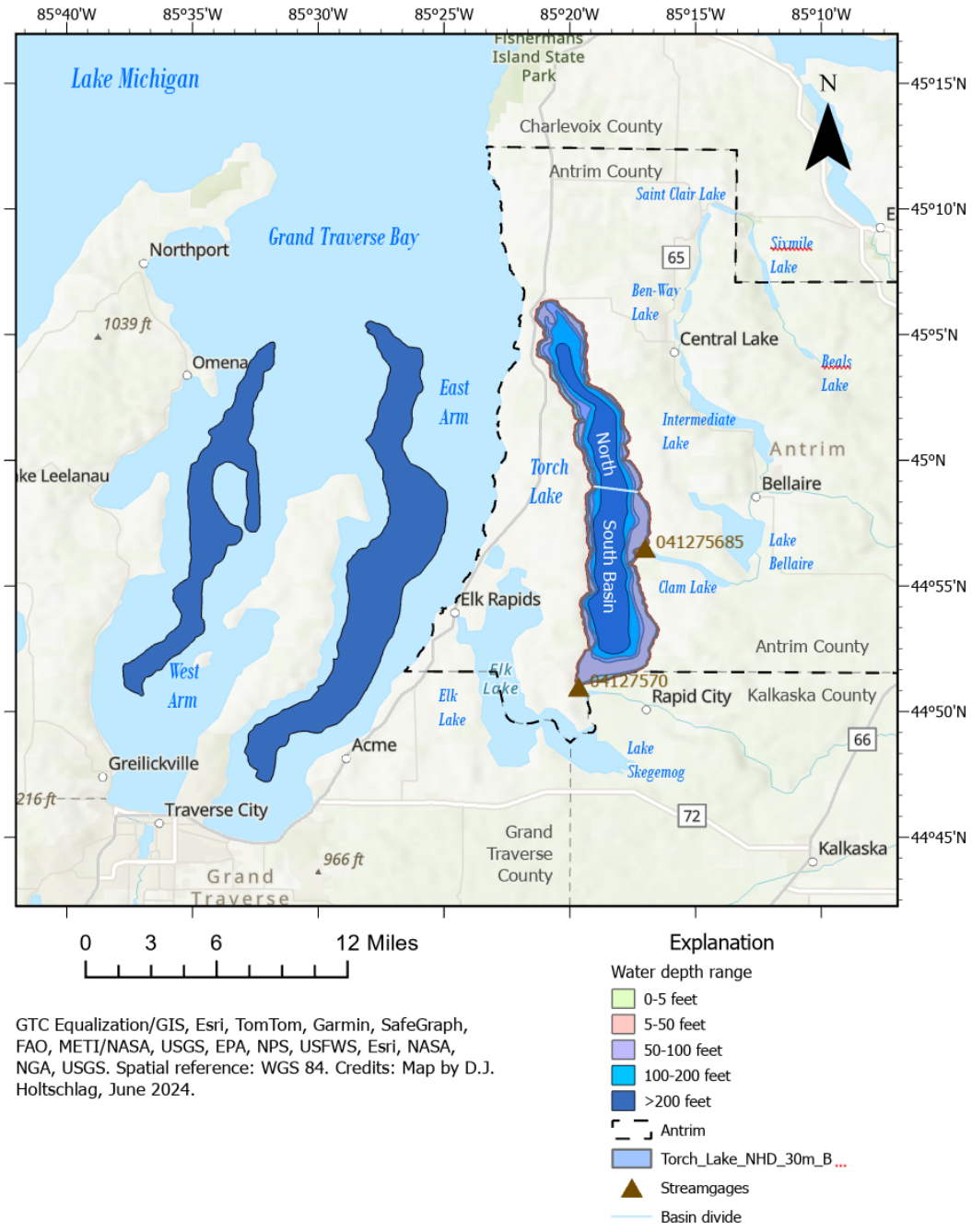

Figure 1. Torch Lake and Grand Traverse Bay vicinity map in Antrim County, Michigan

Data

Data used in this analysis included digital Geographic Information Systems (GIS) data of surface water features compiled in the USGS National Hydrography Dataset (NHD), lake bathymetry data, and satellite imagery from Landsat satellites 5, 7, 8, and 9 for the period from 1984 through 2023. The sources and uses of these data are described in the following paragraphs. Note that Landsat 6 failed to achieve orbit and was never operational.

This report was developed in the RStudio integrated development environment (Posit team 2024, v. 2023.12.1+402) using the R programming language and statistical computing environment (R Core Team 2024, v. 4.3.3). Packages used in the analysis were updated to those current with the corresponding R version. The open-source scientific and technical publishing system Quarto (Allaire and Dervieux 2024) was used to integrate text, images, with model output in a PDF format.

National Hydrography Data

The boundaries of Torch Lake and Grand Traverse Bay are based on the USGS National Hydrography Dataset Plus High Resolution (NHDPlus HR) geospatial dataset (U.S. Geological Survey 2020). NHDPlus HR is a digital vector dataset used by GIS to define the spatial locations of surface waters and is designed to provide comprehensive coverage of surface water data for the U.S. Areal features in NHD representing water features, such as lakes and ponds, are defined by polygons and referenced as a NHD Waterbody. These data are designed to be used in general mapping and in the analysis of surface-water systems.

Within the Torch Lake boundary, a 30-m buffer was extended from the lake boundary (edge of water) inward towards the center of Torch Lake. This masked area was intended to exclude reflectances from overhanging trees, docks, and other features that would not have the same SR as water near the shoreline.

Bathymetry Data

Bathymetry data for Torch Lake was obtained from the Michigan's Open GIS Data Repository for Inland Lake Contours (Michigan Department of Natural Resources 2023). These data were used to define five water-depth intervals of: 0-5 ft, 5-50 ft, 50-100 ft, 100-200 ft, and >200 ft, which provided five concentric zones defining five regions of interest (ROI) in the study area. Reflectances for water depths of 250 feet and greater were included within the $\geq$ 200 foot and greater depth interval. Finally, Torch Lake was subdivided into north and south basins, with areas of about 11.9- and 16.6-mi^2, respectively, that were formed by a line with an azimuth of 100 degrees that transversely bisects the lake through the point 44.98 degrees latitude and -85.30 degrees longitude.

For consistency with the NHD basemap, minor adjustments to the edge of water shown on the Inland Lake Countour map boundaries (U.S. Geological Survey 2020). Also, minor editing of water depth contours were applied for consistency with NHD boundary. Table 2 shows the area and number of pixels bathymetry zones defined for Torch Lake and GTB.

Grand Traverse Bay is west of Torch Lake and receives local inflow, including flows from Torch Lake and other inland sources within Michigan, and is open to and exchanges flow with Lake Michigan. Thus, SR in the GTB may have similarities to SR in both Lake Michigan and nearby inland lakes. Two subareas within the East and West Arms of GTB are defined by the 100-m (328-ft) depth contours (NOAA National Geophysical Data Center 1996). The vertical extent and size of the contoured areas within these areas are comparable to Torch Lake. The maximum contoured depth in Torch Lake of greater then 200 ft, is comparable to the greater than 100-m contour within GTB in that SR is not likely affected by reflectance from the lakebeds. SR in some of the smaller

contour-depth intervals of Torch Lake are likely affected by lakebed reflectance.

Table 2. Water-surface area by waterbody and bathymetry depth intervals

Waterbody	Water Depth Interval	North Basin Area, in square miles	North Basin Maximum number of pixels	South Basin Area, in square miles	South Basin Maximum number of pixels
Torch Lake	0-5 ft	1.0622	4,325	0.7718	3,512
	5-50 ft	1.7424	6,241	4.5353	14,192
	50-100 ft	1.6878	6,007	1.3875	5,005
	100-200 ft	3.1955	10,180	2.4128	7,919
	>200 ft	4.1965	12,551	7.4942	22,038
	Total	11.8843	26,753	16.6016	52,666
		East_Arm	East_Arm	West_Arm	West_Arm
Grand Traverse Bay	>100 m	31.7431	92,818	16.7909	49,606

Landsat Imagery

Figure 2 shows the spatial extents of two scenes obtained on satellite paths 21 and 22 of row 29 in the study area. These scenes were generally imaged between 11:00 AM and 11:30 AM Eastern Standard Time (EST). This timing tends to maximize the scene illumination and minimize the water vapor (haze and cloud conditions). Images of Torch Lake on path 22 are regularly obtained 7 days after images on path 21. Note that Torch Lake has overlapping coverage from scenes obtained along satellite paths 21 and 22, which provides more days of imagery for analysis. Grand Traverse Bay is only imaged on path 22.

Data for Landsat satellites 5, 7, 8, and 9 obtained from 1984 through 2023 were used from all months excluding December, January, and February to help avoid ice-affected conditions. Table 3 shows the range of frequencies defining blue, green, and red bandwidths. Note that bandwidths were constant for Landsat satellites 5 and 7, and for satellites 8 and 9, but differed slightly between satellites 5 and 7, and 8 and 9.

The median SR value of all observed (non-excluded) pixels in a ROI was used as a robust estimate of central tendency of the data. The number of pixels in an ROI was used as a measure of the reliability of the median. The number of valid pixels can vary from 1 to the maximum number of pixels in a ROI. The number of observed pixels within an ROI varied over time with atmospheric conditions at the time of imaging.

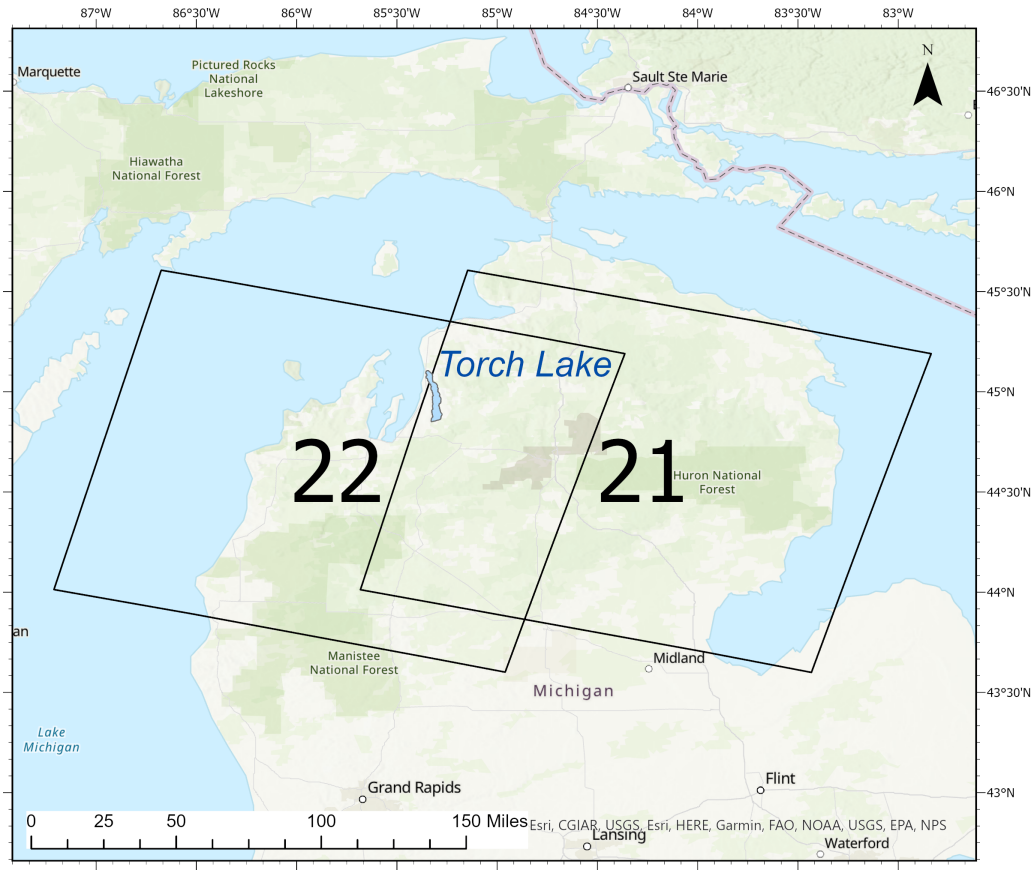

Figure 2. Outlines of Landsat scences associated with paths 21 and 22 of row 29 used in the analysis of surface reflectance of Grand Traverse Bay and Torch Lake in Antrim County, Michigan

Table 3. Changes in band width intervals in surface reflectance data between Landsat satellites

[!h]

Landsat satellite	Color	Band	Wavelength (micro-meters)	Start	End
LT05	Blue	1	0.45-0.52	1984	2011
	Green	2	0.52-0.60	1984	2011
	Red	3	0.63-0.69	1984	2011
LE07	Blue	1	0.45-0.52	1999	2021
	Green	2	0.52-0.60	1999	2021
	Red	3	0.63-0.69	1999	2021
LC08	Blue	2	0.45-0.51	2013	[a]—
	Green	3	0.53-0.59	2013	—
	Red	4	0.64-0.67	2013	—
LC09	Blue	2	0.45-0.51	2023	—
	Green	3	0.53-0.59	2023	—
	Red	4	0.64-0.67	2023	—

Satellite Data Access and Summary Statistics Computations

All satellite data presented in this analysis was accessed and summarized by use of Google Earth Engine (Google 2024a) platform. The GEE interface provides cloud-based access to petabytes of satellite imagery and geospatial datasets GEE also provides a JavaScript code editor and specialized statistical and graphical functions for processing, summarizing, and displaying results in place. Google generously provides free access to GEE for noncommercial and research use. An example of the JavaScripts used to access and process satellite imagery data for this analysis is shown in Appendix 1. Comments within the JavaScript provide additional explanations including masking and statistics computed. JavaScript codes varied for individual satellites. Additional explanation of the GEE functions can be obtained at Google (2024b).

Approach

Distributional Analysis of Surface reflectances

Measured Landsat surface reflectance values used in this report are denoted $\mathcal{R}$. The mean and range of $\mathcal{R}$ from aquatic surfaces is generally less than those associated with land surfaces during ice-free periods. In this report, the empirical cumulative distribution function was analyzed to identify a small range of $\mathcal{R}$ values, defined by endpoints $\mathcal{R}_{min}$ *and* $\mathcal{R}_{max}$, that were likely to contain about 99 percent of the measured $\mathcal{R}$ values for Torch Lake for all bands (eqn. 1).

$$\Pr[\ \mathcal{R}_{min} \leq \mathcal{R}_{bands} \leq \mathcal{R}_{max}] \approx 0.99 \text{ for } \mathcal{R}_{bands} \in \{\mathcal{R}_{blue}, \mathcal{R}_{green}, \mathcal{R}_{red}\} \tag{1}$$

Once the endpoints were determined, $\mathcal{R}$ was rescaled to $\mathring{\mathcal{R}}$, which is defined on the interval [0,1] (eqn. 2).

$$\mathring{\mathcal{R}} = \frac{\mathcal{R} \mid (\mathcal{R}_{min} \leq \mathcal{R} \ \leq \ \mathcal{R}_{max}) - \mathcal{R}_{min}}{\mathcal{R}_{max} - \mathcal{R}_{min}} \tag{2}$$

Following rescaling, a nonlinear transform was applied that is commonly referred to as a gamma correction (eqn. 3). This transform exponentiates the rescaled values of reflectance with a constant less than 1 to reduce the skew of (help normalize) the distribution. The transform shifts the mode of the probability density function to the right and tends to make the tails of the density more symmetrical. The transform preserves the [0,1] range of the rescaled reflectance values.

The intensity of $\dot{\mathcal{R}}$ for each primary color band were combined using the R function `rgb()` to describe a color (as a single hexidecimal code) (R Core Team 2024). Visually, the transformed values produce a lighter tone than rescaled values.

$$\dot{\mathcal{R}} = \mathring{\mathcal{R}}^{\gamma} \tag{3}$$

Atmospheric Bias Adjustment

Although the maximum number of pixels is a constant based on the area of the region of interest (table 2), the number of measurable pixels is affected by atmospheric conditions that vary widely among images. An analysis was conducted to reduce the possible bias in $\dot{\mathcal{R}}$ based on the differences between observed number of pixels in a ROI and the maximum number of pixels in the regions of interest.

Katsaros et al. (1985) indicated that the albedo for cloudy skies may be greater than the albedo for clear skies due to reflections back from the water surface that were re-reflected from the undersides of clouds. To investigate the possibility that a bias may be associated with cloudiness, parameters were estimated for a decay function (eqn. 4). In this function, cloudiness was indexed as the percentage of pixels measured *(mea.pixel.pct)* after eliminating pixels indicated as clouds, cloud shadows, or ice using the *QA_PIXEL* band. The percentage was based on the number of measured pixels in a particular scene divided by the maximum number of pixels measured in the ROI for all scenes. The maximum percentage (100) of measurable pixels is denoted as *mea.pixel.100*.

$$\hat{\dot{\mathcal{R}}}(\ mea.pixel.pct \mid a, b\ ) = a \cdot e^{-b \ \cdot \ mea.pixel.pct} \tag{4}$$

where a and b are estimated parameters, and
e is Euler's number (≈ 2.71828).

Parameters *(a,b)* for decay functions were estimated by use of the nonlinear least squares analysis using the R function `nls()` in the {stats} package (R Core Team 2024) and data for specific regions of interest. An equation was considered statistically significant if the 95-percent confidence intervals about both parameters' estimates excluded zero. If significant, a bias adjustment was computed using equation 5.

$$\ddot{R} = \dot{R} \; + \; \hat{\dot{\mathcal{R}}}(mea.pixel.100|a,b) \; - \; \hat{\dot{\mathcal{R}}}(mea.pixel.pct|a,b) \tag{5}$$

Generalized Additive Modeling

Generalized Additive Models (GAM) are statistical models that contain parametric and smooth components for estimating a continuous response variable (Wood, S.N. 2006). The response variables in this analysis were the $\ddot{\mathcal{R}}$ for each color band of visible light. Parametric and smooth terms are discussed below along with criteria for model estimation and assessment.

The form of the GAM specified for Torch Lake is

$$\begin{aligned} gam.object \leftarrow gam(\ddot{\mathcal{R}} \sim\; & SAT + Depth + Path + Basin + && \text{(Parametric)} \\ & s(day.of.year,\ bs = \ "cr") + s(day.19840301,\ bs = \ "cr")\ , && \text{(Smooth)} \\ & gamma = 1.4, weight = sqrt(mea.pixel.pct),\ data = TL\_LSAT) && \text{(Ancillary)} \end{aligned}$$

The *gam.object* contains 49 elements computed by the GAM software, which include `fitted.values`, here $\hat{\ddot{\mathcal{R}}}$, and model *residuals*, denoted ϵ, model parameters, and statistics. The residuals are assumed to be independent and identically distributed (i.i.d) random variables that are normally distributed with mean zero and variance σ_ϵ^2 (eqn. 6).

$$\ddot{\mathcal{R}} = \hat{\ddot{\mathcal{R}}} + \epsilon, \text{ such that the } \epsilon_i \sim N(0, \sigma_\epsilon^2) \text{ and i.i.d} \tag{6}$$

Parametric Terms

Parametric terms describe the statistical association between an explanatory and response variable by use of a single set of parameters. In this analysis, the intercept term and factor variables are included as parametric terms. The intercept term adjusts model estimates for the average level of the response variable based on a single parameter. Factor variables adjust model estimates for two or more ordered levels of a factor variable. The first level of a factor variable provides a reference level of zero for all other levels within the factor variable. With this convention, a parameter value of zero is not listed in the output results. A set of parameters for each of the remaining levels is estimated along with statistics indicating their apparent significance.

Parametric terms are specified in a GAM model similar to the way explanatory variables are specified in a multiple linear regression equation. In these GAM models, an intercept term and factor variables were the only parametric terms used. An intercept term is estimated by default. Factor variables with predefined levels were defined for satellites (SAT), water-depth interval (Depth), satellite path (Path), and subset of the lake (Basin). In a GAM model the parametric terms would be specified as shown in equation *Parametric*, where gam.object is a container for the computed outputs.

Satellite Factor

A satellite factor variable (*SAT*) was included in the GAM models to harmonize the mean levels of response for different Landsat satellites. This factor variable was included in response to concerns that inclusion of Landsat 5 and 7 with Landsat 8 and 9 data would cause an erroneous negative trend in surface reflectances. Some of this possible bias may be associated with changes in band width intervals between the two sets of Landsat data (table 3). In GAM summary output tables, satellite parameters have the prefix of `SAT` and suffixes `LT07`, `LC08` and `LC09`, respectively, indicating how the mean level of a response changed from the implied reference level of zero for `LT05`.

Water-Depth Factors

Bathymetric data in the form of contour intervals were available for both Torch Lake and Grand Traverse Bay. Contour intervals indicate the depth below the average water surface. Water depth is thought to affect the combined surface reflection from both the water surface and the lakebed. The available bathymetry data for Torch Lake were used to define five water-depth intervals for factor variable *Depth*. In GAM summary output tables, parameters for water-depth intervals have the prefix *Depth* and suffixes of `5-50, 50-100, 100-200,` and `>200` ft for the four deeper water depth intervals. The parameters indicate how the mean level of response changed from the reference level of zero implied for water depth interval from `0-5` ft. For Grand Traverse Bay, however, variations in surface reflectance with water depth interval were not investigated. As a reference for Torch Lake, however, one depth interval of 100-m and greater was defined, which was assumed to be indicative of surface reflectance from only the water surfaces rather than the lakebed.

Basin Factors

Torch Lake is elongated in the north-south direction, which may limit mixing of sediments and nutrients associated with streamflow because both inflows and outflows occur in the south basin. Thus, any changes in reflectance associated with streamflow components may not be expressed equally in the two basins.

The factor variable *Basin* has two levels to represent possible differences in mean reflectances for the south basin relative to the reference level of zero implied for the North basin. Similarly, in Grand Traverse Bay, two basins were defined by the 100-m and deeper water-depth contour intervals: one in the East Arm and a second in the West Arm. Waters in the East and West Arms may not be fully mixed and the altitude and azimuth angles of reflected light may differ due to the east-west separation of the two basins. The East Arm is the reference level for Grand Traverse Bay.

Satellite Path Factors

Torch Lake was imaged by Landsat satellites on paths 21 and 22. Given that the two paths have different altitude and azimuth angles, the mean reflectances for the two paths may differ. Thus, the factor variable *Path* was included in the Torch Lake GAM. Here, path 21 served as the reference level of zero. Grand Traverse Bay was only imaged on path 22, so Path factor variable was not used.

Smooth Terms

Smooth terms are formed by smoothing spline functions g of a co-variate, x, that provides an estimate of the relation between the magnitude of the co-variate on the magnitude of the response variable, $\ddot{\mathcal{R}}$. The adjective *smooth* implies that the spline does not match each response value exactly, but attempts to minimize the sum of squared residuals formed as $\ddot{\mathcal{R}} - g(x) = \epsilon$, left hand side term in equation (7), without letting g get too wiggly as described by integrating the second derivative of the function $g(s)''$, in right hand side term (eqn. 7).

$$\sum_{i=1}^{n} \left(\ddot{\mathcal{R}}_i \ - g(x_i) \right)^2 + \lambda \int \ g''(x_i)^2 \ dx \tag{7}$$

The trade-off between minimizing residuals squared (model fit) and wiggliness is affected by the λ parameter. In general, a higher *gamma* parameter as an ancillary term in the model specification is associated with a higher λ value, a greater penalty for wiggles, and fewer effective degrees of freedom (edf) of the smooth term. Wood (2006) notes that a γ value of 1.4 tends to correct an occasional overfitting problem without compromising model fit.

Smoothing splines provide more stable approximations of a function over an interval, like the domain of $\ddot{\mathcal{R}}$, than polynomial bases, which may be preferred for point estimation. The basis function used in the smooths were cubic regression (cr) splines because they have directly interpretable parameters (Wood, S.N. (2006)).

Smooth terms are specified in a GAM model for seasonal (*day.of.year*) and trend (*day.19840301*) components. The smooth terms are distinguished from parametric terms by enclosing the variable names and associated arguments in a pair of parenthesis preceded by the letter 's' (eqn. *Parametric*). The smooth specification can be extended to compute the smooth by levels of a factor variable. For example *s(day.of.year, by = Depth)* will compute seasonal smooths for each water-depth interval. In addition to specifying variables, the smooth can specify the type of basis (*bs*) function within the parenthesis. For example, inserting the string *bs = 'cr'*, specifies that the basis function would be a penalized cubic regression spline (Wood, S.N. (2006)).

Seasonal Components

A seasonal variable *day.of.year* was computed as the day of the year that a satellite image was acquired. The day of the year is the number of days in the year beginning with January 1 as 1. Given that data from December, January, and February were excluded, the minimum and maximum day numbers for Torch Lake were 60 and 334, respectively.

Local Levels and Trends

A local-level variable *day.198403001* was computed as the number of days since February 29, 1984, making March 1, 1984 day 1. The date of the first image used in the analysis occurred on March 25, 1984. The last date of satellite imagery used in this analysis was November 20, 2023. A local-level component may not be monotonically increasing or decreasing during the entire period of analysis, but still show a consistent pattern within an extended subinterval. When the pattern in local-level variations is considered systematic it is described as a trend within a specified subinterval.

Ancillary Terms

Model terms (eqn. *Ancillary*) were completed by specifying *gamma*, which affects the smoothness of the seasonal and local level terms, *weight*, which provides a measurement weighting factor, and a *data*, which is a data structure

that contains the variables in the parametric and smooth terms. A *gamma* value of 1.4 was specified, rather than a default value of 1, to help avoid overfitting the model without compromising model fit. The measurement *weight* was the square root of the percent of possible pixels in the region of interest assuming that a median value that was based on more pixels woould be more reliable, and *data* was an *R* data.frame containing the model variables.

Model Assessment

The primary numerical metric for assessing overall model performance is the sample coefficient of determination or r^2 value, which is the proportion of the variability in $\ddot{\mathcal{R}}$ data that is described by the explanatory variables in the model. Commonly used descriptive categories for ranges of r^2 values are: <0.3, which indicates a Very Weak relation; $0.3 \leq r^2 < 0.5$ indicates a Weak relation; $0.5 \leq r^2 < 0.7$ indicates a Moderately Strong relation, and $r^2 \geq 0.7$ indicates a Strong relation (Moore, Notz, and Flinger 2011).

In addition to the r^2 value, linear components metrics include the parameter estimate, its standard error, an associated Student's *t*-value, and the probability of a greater absolute value of *t* (Pr(>|t|) given the null hypothesis that the true value of the parameter is zero. The smaller this probability is, the more likely the parameter is statistically significant. For factor variables, the parameter level estimates are relative to the reference level for the factor as a mean difference. For the satellite factor (SAT) the reference level is LT05, which is set to zero (and is not displayed in summary tables). Statistical significance between factor levels are all referenced to LT05. Thus, for example, both LC08 and LC09 may be significantly different from LT05, but not from each other. If reported factor level parameters are negative, it means that the responses were generally lower than the response for the reference level. Other factor variables include the satellite path, where path 21 provided the reference level, and the water-depth interval, where the 0-5 ft interval provided the reference level.

Metrics for the smooth components include the Effective Degrees of Freedom (*edf*) and the Reference Degrees of Freedom (*Ref.df*). The *edf* relates to the flexibility of the model in which a higher *edf* means the model is more flexible and can capture more complex patterns. A very high value of *edf* relative to the number of data points might indicate an overfitting of the model, while a very low value might indicate underfitting. The *edf* is not always an integer value because it reflects the sum of the estimated eigenvalues of the smoothing parameter matrix. The *Ref.df*, on the other hand, is the degrees of freedom for the smooth terms in a comparable parametric model. In polynomial regression, for example, the *Ref.df* would be the number of estimated model parameters. Thus, the *Ref.df* presents a maximum value for the *edf*, while their difference reflects the relative reduction in degrees of freedom due to smoothing. The statistical significance for the smooth terms, which have multiple degrees of freedom, were described by the *F* statistic and the corresponding probability of a greater (non-negative) F value (Pr(>F)) given that the null hypothesis that all parameters in the term were equal to zero.

Graphical evidence of the statistical significance of the smooth terms was generated by plotting contents from the `gam.object`. For example, in `R`, the command `plot(gam.object)` will plot each smooth component over the domain of the function along with a 95-percent confidence interval for each smooth term in the model. The mean value of all smooth term estimates equals zero. Segments within the domain of the function were the 95-percent confidence interval does not intersect zero are areas of statistical differences.

Results

Torch Lake

Table 4 shows the number of images analyzed by basin and water-depth interval. The median number of images in each region of interest is 1,027. The number of images per satellite varies primarily with the length of the satellite record with LE05 having the longest and LC09 having the shortest period of data.

Table 4. Number of satellite images of Torch Lake by basin and water depth interval

	North Basin Water Depth Intervals, in feet					South Basin Water Depth Intervals, in feet				
Satellite	0-5	5-50	50-100	100-200	>200	0-5	5-50	50-100	100-200	>200
LT05	427	426	425	421	420	459	461	443	447	441
LE07	392	399	399	396	395	398	410	393	396	398
LC08	174	175	172	173	170	182	185	178	178	181
LC09	15	16	16	16	16	18	19	18	18	18
Total	1008	1016	1012	1006	1001	1057	1075	1032	1039	1038

Table 5. Maximum number of pixels in Torch Lake regions of interest by basin and water depth interval

	North Basin Water Depth Intervals, in feet					South Basin Water Depth Intervals, in feet				
Satellite	0-5	5-50	50-100	100-200	>200	0-5	5-50	50-100	100-200	>200
LT05	4325	6241	6007	10180	12551	3512	14192	5005	7919	22038
LE07	4325	6241	6007	10180	12551	3512	14192	5005	7919	22038
LC08	4325	6241	6007	10180	12551	3512	14192	5005	7919	22038
LC09	4314	6241	6007	10180	12551	3474	14101	5005	7919	22038

Distribution Analysis

Figure 3 shows the cumulative distribution function for the blue, green, and red bands of $\mathcal{R}$ between a surface reflectance of 7,100 and 13,200. the red band had the lowest surface reflection in all depth intervals. Reflectance in all bands also shifted to the left at greater depths, with the green band shifting more to the left than the blue band as evidenced by generally lower reflectance in the green band relative to the blue band at greater depths. Little change in the relative positions of the blue, green, and red bands occurred at depth intervals having a lower bound of 50 ft.

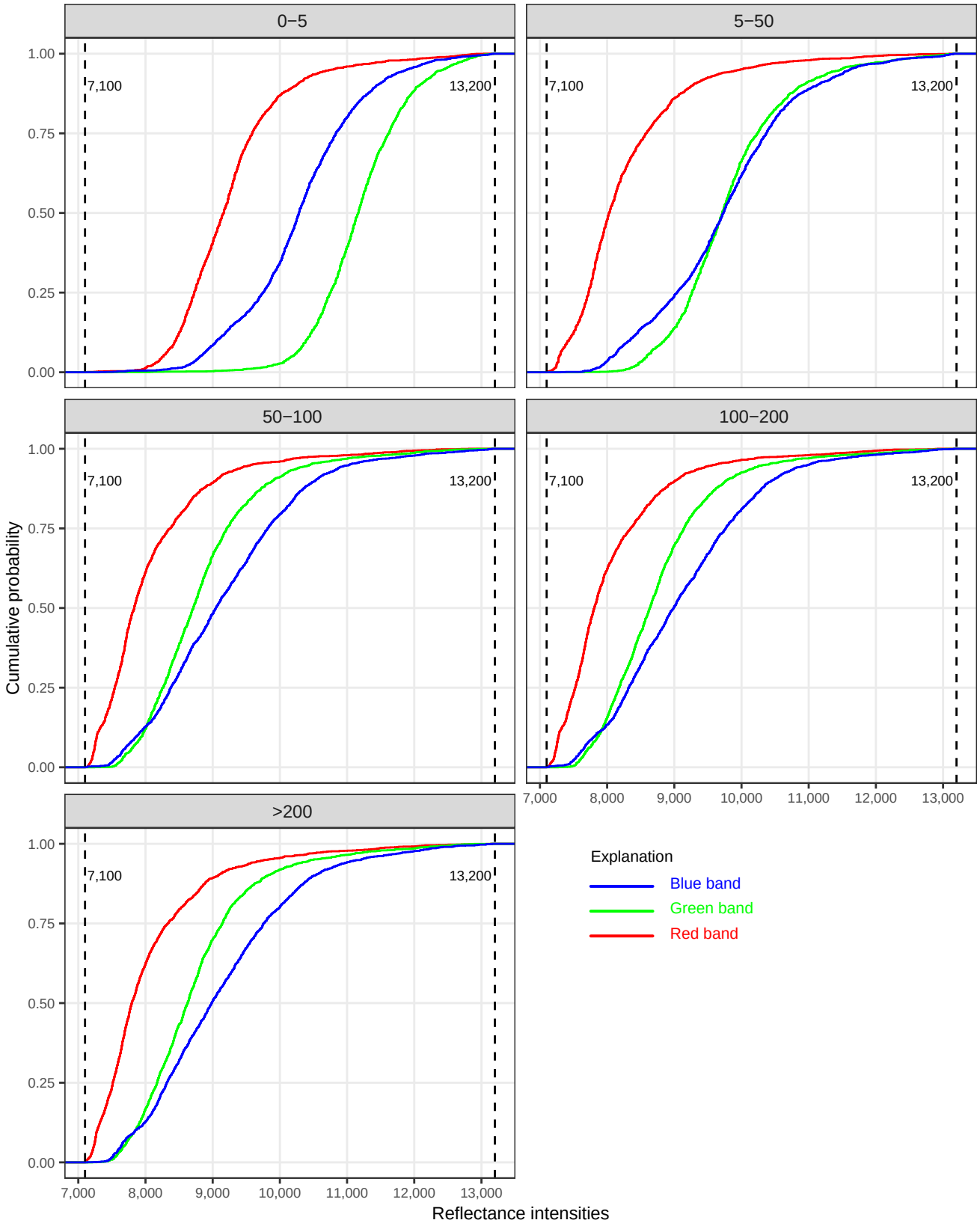

Figure 3. Cumulative distributions of surface reflectance data for Torch Lake by bathymetry interval and color band

Figure 4 shows the empirical probability densities of rescaled and transformed surface reflectances in blue, green, and red bands for Torch Lake by water-depth interval. Measured reflectances were rescaled using eqn. 8, to produce reflectances that ranged from [0,1]. The rescaling parameters were based on minimum and maximum reflectances that contained 99 percent of the measured reflectances. The resulting probability densities are generally right skewed, particularly in the red band. The rescaled values were then exponentiated by constants less than one (table 6) to more closely approximate a normal probability density using eqn. 3. The constants were selected manually to produce more symmetrical densities while preventing band modes from overlapping. The transform also preserved the range from [0,1].

$$\mathring{\mathcal{R}} = \frac{\mathcal{R} - 7,100}{13,200 - 7,100} \tag{8}$$

Table 6. Exponents used in gamma transform of rescaled surface reflectances by band and depth

Color	Water-depth interval		
band	0-5 ft	5-50 ft	>50 ft
blue	0.625	0.575	0.450
green	0.575	0.875	0.540
red	0.700	0.700	0.590

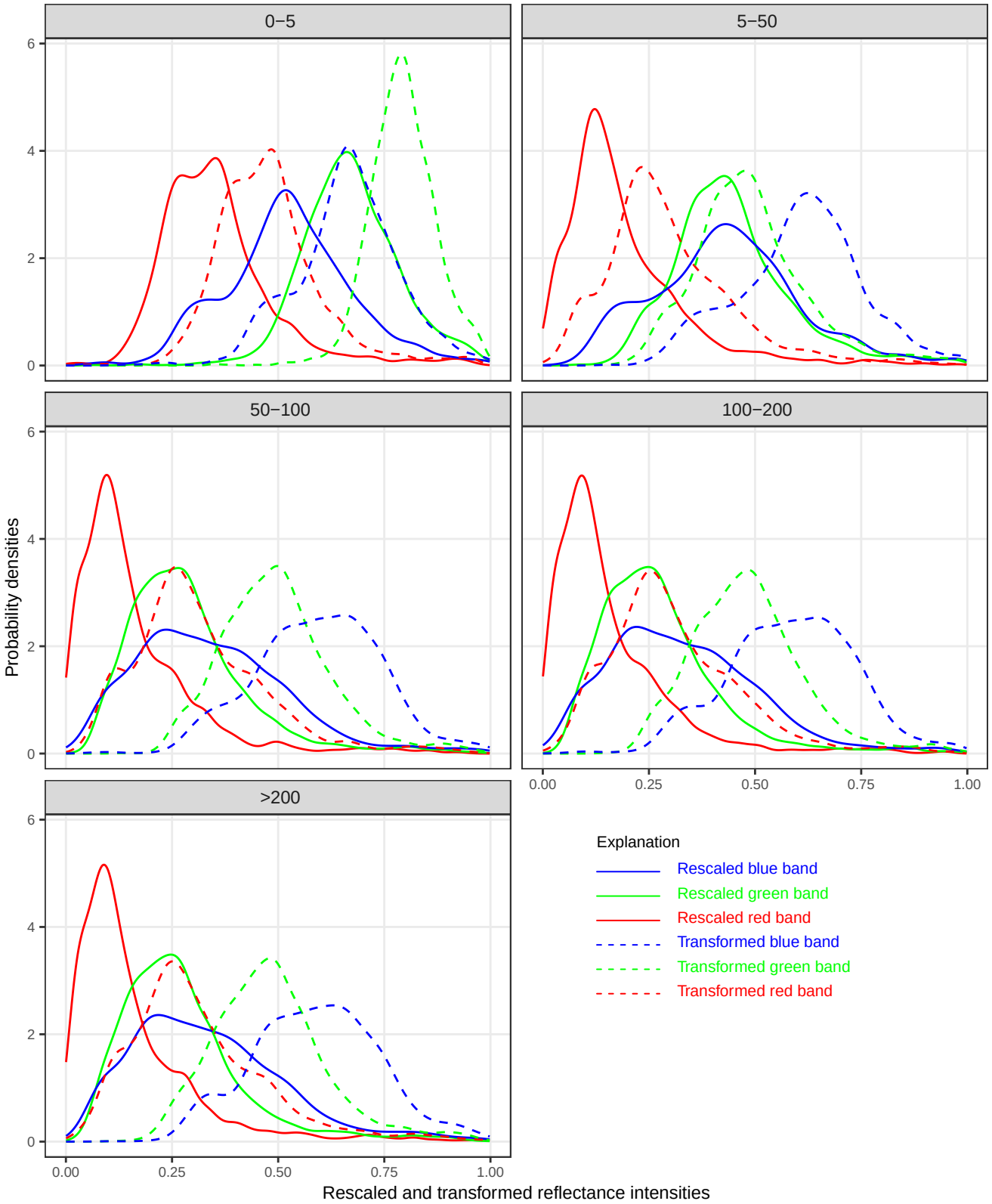

Figure 4. Probability densities of rescaled and transformed blue, green, and red bands of surface reflectance intensities by bathymetry intervals for Torch Lake, Michigan

Figure 5 shows the estimates of visible light reconstructed from intensities of rescaled and transformed surface reflectances in the blue, green, and red bands. Note that the transforms shift the mode of the reflectance frequencies to the right (fig. 4), resulting in a lighter coloration. This transition from the intensities of individual primary (blue, green, and red) bands to color is approximate. Visible light is generally thought to span wavelengths from about 0.38 to 0.75 micrometers (10^{-6} meters). Landsat 5 and 7 and Landsat 8 and 9 partly span different parts of this spectrum (table 3). As bands average frequencies over intervals that do not completely span the visible spectrum, neither image reconstructed from individual bands can represent the true color transformation.

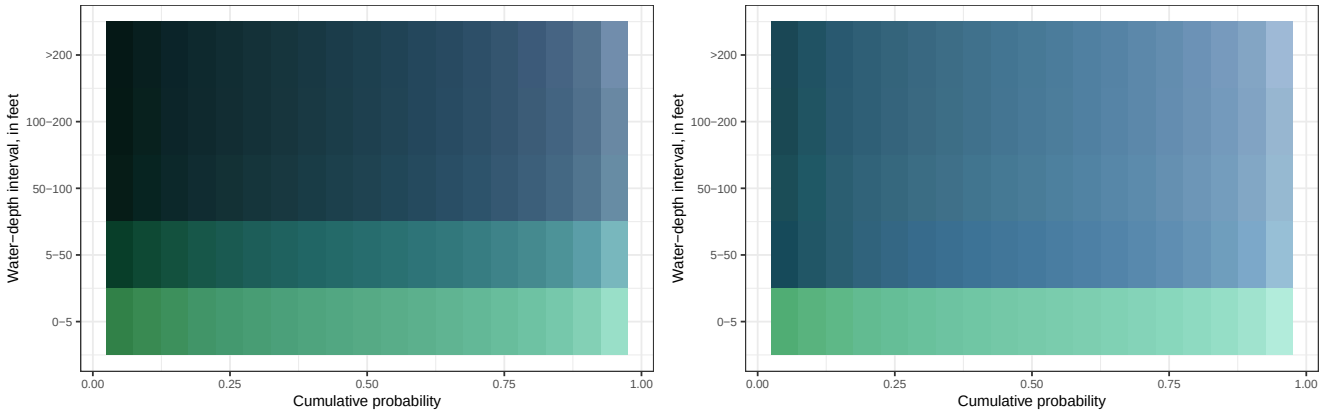

(a) Rescaled band intensities

(b) Transformed band intensities

Figure 5. Light reflectance probabilities from blue, green, and red bands of surface reflectance by water-depth intervals for Torch Lake, Michigan

Atmospheric Bias Adjustment

Table 7 shows the estimated parameters and uncertainties for the decay functions by band and water-depth intervals and figs. 6, 7, and 8 show the corresponding plotted information. Note that in the figures, the y-intercepts (dashed lines) are the minimum values of the decay functions at 100 percent of pixels measured, which is labelled in the table as `predict 100-%`. The value of `predict 100-%` generally decreases with increasing water depth intervals for all bands. The `bias adjustment` is the vertical distance between the decay function at measured percentage of pixels `predict mea-%`, and at `predict 100-%`. Values of the `bias adjustment` generally increased with increasing depth for all bands.

Table 7. Parameters for nonlinear equation relating reflectance intensity decay with percent of measured pixels in Torch Lake water-depth intervals

			Water depth intervals, in feet				
Band	Parameter	Statistic	0-5	5-50	50-100	100-200	>200
Blue	a	estimate	0.6999***	0.6850***	0.6740***	0.6651***	0.6990***
		std.error	(0.0058)	(0.0067)	(0.0071)	(0.0073)	(0.0075)
	b	estimate	0.00091***	0.00198***	0.00200***	0.00200***	0.00260***
		std.error	(0.00012)	(0.00015)	(0.00015)	(0.00016)	(0.00015)
	N		1976	2018	1989	1982	1959
	predict	100-%	0.6388	0.5618	0.5520	0.5448	0.5392
	bias	adjustment	0.0512	0.1182	0.1180	0.1152	0.1508
Green	a	estimate	0.8063***	0.602***	0.5934***	0.5790***	0.5958***
		std.error	(0.0037)	(0.006)	(0.0061)	(0.0062)	(0.0066)
	b	estimate	2.8e-04***	0.00342***	0.00291***	0.00289***	0.00328***
		std.error	(6.6e-05)	(0.00016)	(0.00015)	(0.00016)	(0.00016)
	N		1964	2033	2001	2008	1994
	predict	100-%	0.7843	0.4280	0.4436	0.4335	0.4292
	bias	adjustment	0.0157	0.1720	0.1464	0.1365	0.1608
Red	a	estimate	0.5556***	0.447***	0.4543***	0.4563***	0.4897***
		std.error	(0.0055)	(0.007)	(0.0077)	(0.0078)	(0.0081)
	b	estimate	0.00252***	0.00712***	0.00622***	0.00640***	0.00731***
		std.error	(0.00015)	(0.00028)	(0.00028)	(0.00028)	(0.00027)
	N		2022	2038	1979	1975	1965
	predict	100-%	0.4317	0.2191	0.2440	0.2405	0.2358
	bias	adjustment	0.1183	0.2209	0.2060	0.2095	0.2442

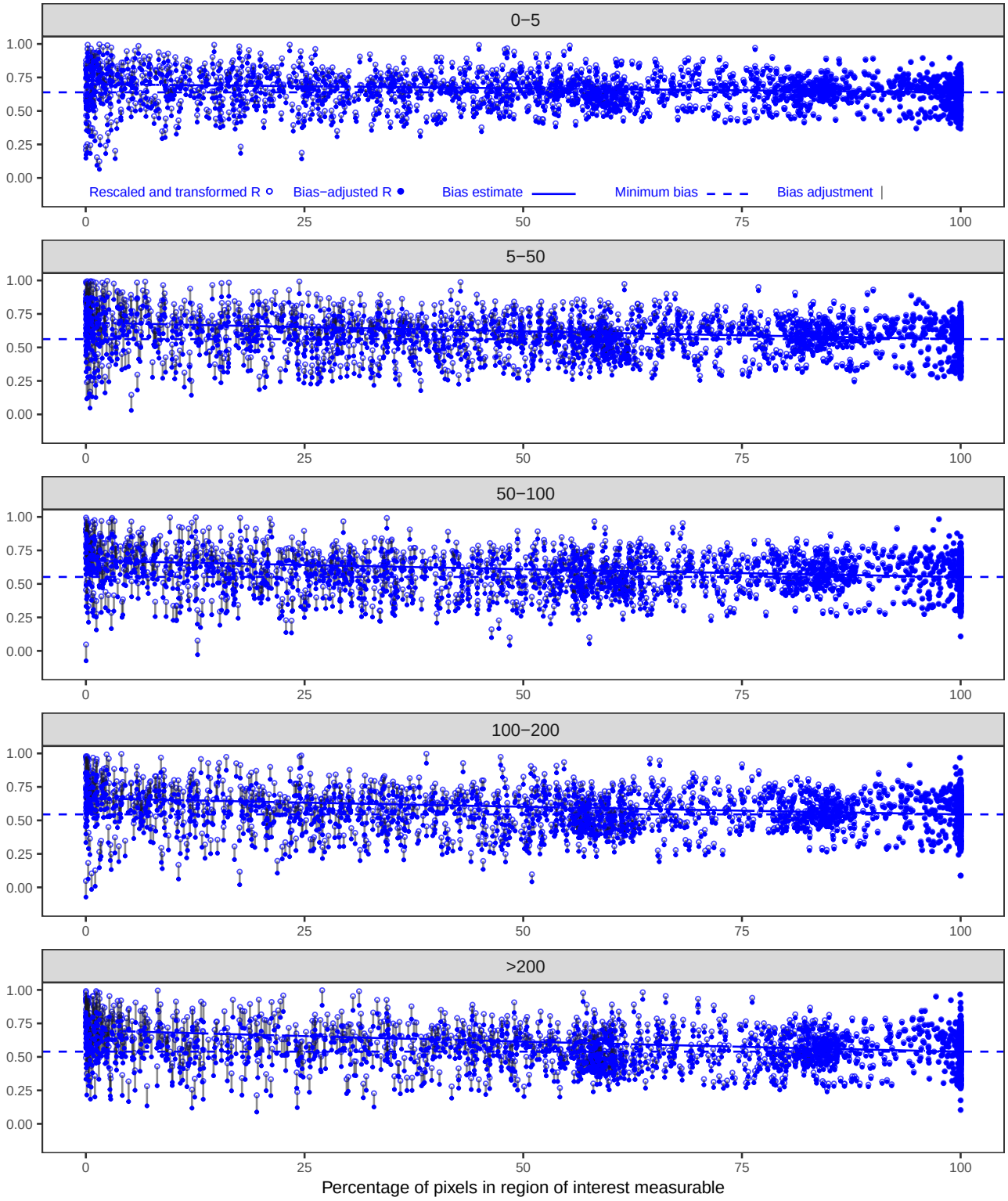

Figure 6. Surface reflectivity of blue band of visible light from all water-depth intervals on Torch Lake in Antrim County, Michigan

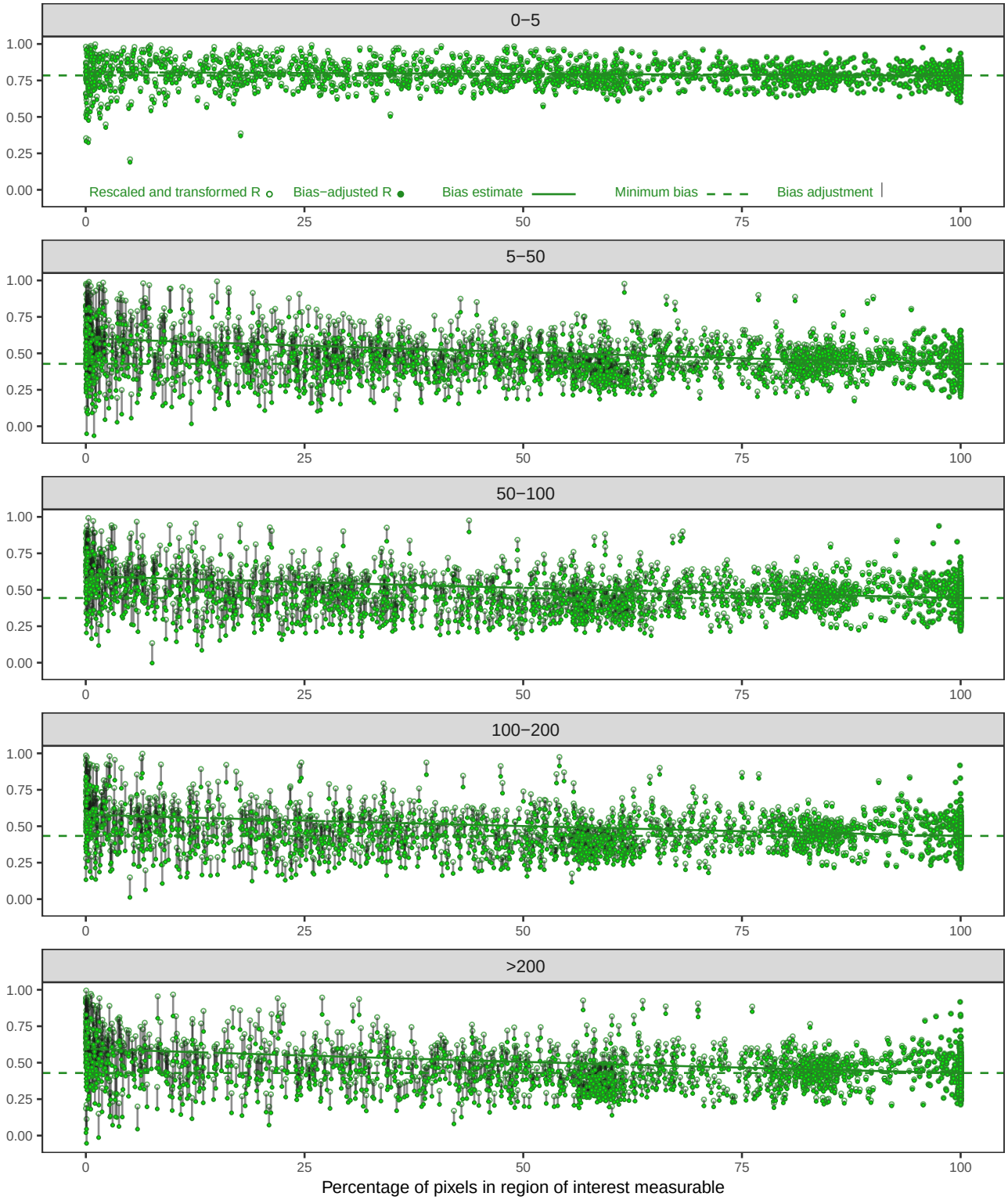

Figure 7. Surface reflectivity of the green band of visible light from all water-depth intervals on Torch Lake in Antrim County, Michigan

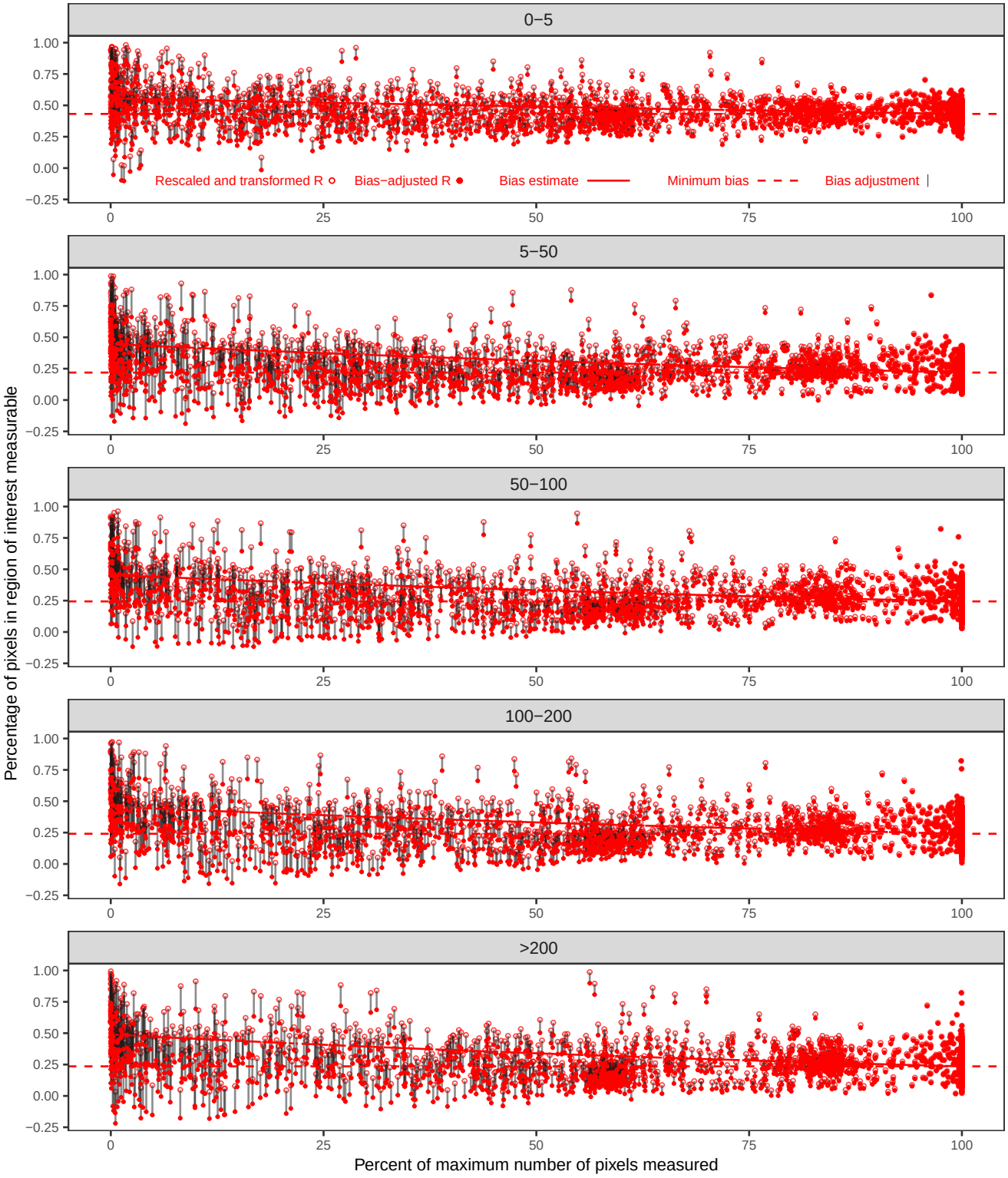

Figure 8. Surface reflectivity of the red band of visible light from all water-depth intervals on Torch Lake in Antrim County, Michigan

Generalized Additive Modelling

Results for GAM modeling of surface reflectances from blue, green, and red bands are shown in tables 8, 9, and 10. Models for all bands included a parametric term for an intercept, a factor variable for satellites (SAT, referenced to LT05), a factor variable for depth intervals (Depth, referenced to 0-5 ft), a factor variable for basin (Basin, referenced to North), and a factor variable for satellite path (Path, referenced to 21). Smooth terms for both seasonal and local level components were computed by depth intervals. The model r-squared values for the corresponding bands was 0.740, 0.815, and 0.638, indicating a moderately strong to strong relation to the $\ddot{\mathcal{R}}$ reflectances. Parametric and smooth terms were indicated as highly significant (p-value < 0.001) for all bands.

Parameters for the satellite factor (SAT) indicate that satellites LE07, LC08, and LC09 all had lower mean reflectances than reference satellite LT05 for all bands. Moreover, the parameters for satellites LC08 and LC09 were less than the departures for LE07. The negative parameters help reduce or eliminate a false downward trend in reflectances (Rocchio, Laura E.P. 2023) that would otherwise be indicated if the SAT variables were not present.

Table 8. Generalized additive model output for blue band reflectance from Torch Lake in Antrim County, Michigan

Component	Term	Estimate	Std Error	t-value	p-value	
A. parametric coefficients	(Intercept)	0.67291	0.00227	296.32	0.000000	***
	SAT LE07	-0.02602	0.00203	-12.81	0.000000	***
	SAT LC08	-0.15025	0.00322	-46.65	0.000000	***
	SAT LC09	-0.15405	0.00799	-19.28	0.000000	***
	Depth 5-50	-0.07933	0.00220	-36.07	0.000000	***
	Depth 50-100	-0.09041	0.00219	-41.19	0.000000	***
	Depth 100-200	-0.09782	0.00219	-44.60	0.000000	***
	Depth >200	-0.10283	0.00219	-47.01	0.000000	***
	Basin South	-0.01389	0.00138	-10.05	0.000000	***
	Path 22	0.02081	0.00139	14.92	0.000000	***
Component	**Term**	**edf**	**Ref. df**	**F-value**	**p-value**	
B. smooth terms	s(day.of.year):Depth 0-5	6.47583	7.61189	38.81	0.000000	***
	s(day.of.year):Depth 5-50	7.05045	8.11028	53.14	0.000000	***
	s(day.of.year):Depth 50-100	8.09241	8.78083	165.47	0.000000	***
	s(day.of.year):Depth 100-200	8.27139	8.85560	194.29	0.000000	***
	s(day.of.year):Depth >200	8.40722	8.90268	202.38	0.000000	***
	s(day.19840301):Depth 0-5	5.80797	6.87562	66.64	0.000000	***
	s(day.19840301):Depth 5-50	7.81740	8.58542	121.64	0.000000	***
	s(day.19840301):Depth 50-100	8.20989	8.80004	72.96	0.000000	***
	s(day.19840301):Depth 100-200	8.13490	8.76403	68.04	0.000000	***
	s(day.19840301):Depth >200	8.29248	8.83705	65.51	0.000000	***

Adjusted R-squared: 0.740, N: 9924, Significance codes: '***' = <0.001, '**' = <0.01, '*' = <0.05

Like the SAT variable, the factor variable for water-depth interval (Depth) had negative parameters for all bands relative to the reference interval from 0-5 ft. Differences between parameters for shallow ($ $5 ft) and deeper waters were attributed to the effect of less lakebed reflectances.

Table 9. Generalized additive model output for green band reflectance from Torch Lake in Antrim County, Michigan

Component	Term	Estimate	Std Error	t-value	p-value	
A. parametric coefficients	(Intercept)	0.80188	0.00248	323.03	0.000000	***
	SAT LE07	-0.04129	0.00222	-18.64	0.000000	***
	SAT LC08	-0.09325	0.00352	-26.52	0.000000	***
	SAT LC09	-0.06213	0.00888	-6.99	0.000000	***
	Depth 5-50	-0.35853	0.00240	-149.63	0.000000	***
	Depth 50-100	-0.34450	0.00239	-144.06	0.000000	***
	Depth 100-200	-0.35456	0.00239	-148.53	0.000000	***
	Depth >200	-0.35761	0.00238	-150.29	0.000000	***
	Basin South	-0.01246	0.00150	-8.30	0.000000	***
	Path 22	0.03919	0.00151	25.87	0.000000	***
Component	**Term**	**edf**	**Ref. df**	**F-value**	**p-value**	
B. smooth terms	s(day.of.year):Depth 0-5	5.64638	6.78945	10.46	0.000000	***
	s(day.of.year):Depth 5-50	6.68349	7.79957	11.11	0.000000	***
	s(day.of.year):Depth 50-100	7.87045	8.66943	46.08	0.000000	***
	s(day.of.year):Depth 100-200	8.06622	8.76865	57.23	0.000000	***
	s(day.of.year):Depth >200	8.36352	8.88847	60.30	0.000000	***
	s(day.19840301):Depth 0-5	8.27441	8.82880	12.08	0.000000	***
	s(day.19840301):Depth 5-50	7.95956	8.66936	39.50	0.000000	***
	s(day.19840301):Depth 50-100	7.81409	8.58278	35.76	0.000000	***
	s(day.19840301):Depth 100-200	8.04202	8.71551	35.67	0.000000	***
	s(day.19840301):Depth >200	8.07267	8.73192	36.48	0.000000	***

Adjusted R-squared: 0.815, N: 10000, Significance codes: '***' = <0.001, '**' = <0.01, '*' = <0.05

For the Basin variable, the south basin had slightly lower reflectances in the blue and green bands, but higher reflectances in the red band. Differences in reflectances may be attributable to inflow from Clam River and outflow from Torch River, which are both located in the south basin, that transported various sediment or organic particles that were differentially reflected or absorbed by the three frequency bands.

Inspection of fig. 2 shows that the centroid of scene 22 is closer to Torch Lake than the centroid of 21, in which Torch Lake is located on the western edge of the scene. These differences imply the sun elevations were higher for scene 22 images than 21 images. Thus albedo (and reflectivity) map have been greater during partly cloudy conditions (Katsaros et al. 1985), which were based on the percent of measurable pixels commonly obtained.

Table 10. Generalized additive model output for red band reflectance from Torch Lake in Antrim County, Michigan

Component	Term	Estimate	Std Error	t-value	p-value	
A. parametric coefficients	(Intercept)	0.42836	0.00278	154.26	0.000000	***
	SAT LE07	-0.05140	0.00248	-20.75	0.000000	***
	SAT LC08	-0.14800	0.00377	-39.28	0.000000	***
	SAT LC09	-0.13037	0.00858	-15.20	0.000000	***
	Depth 5-50	-0.21194	0.00273	-77.65	0.000000	***
	Depth 50-100	-0.18874	0.00273	-69.10	0.000000	***
	Depth 100-200	-0.19180	0.00273	-70.30	0.000000	***
	Depth >200	-0.19440	0.00272	-71.48	0.000000	***
	Basin South	0.01632	0.00172	9.49	0.000000	***
	Path 22	0.07446	0.00173	42.97	0.000000	***
Component	**Term**	**edf**	**Ref. df**	**F-value**	**p-value**	
B. smooth terms	s(day.of.year):Depth 0-5	4.50727	5.53519	32.78	0.000000	***
	s(day.of.year):Depth 5-50	5.44014	6.57079	54.42	0.000000	***
	s(day.of.year):Depth 50-100	5.04569	6.13981	54.40	0.000000	***
	s(day.of.year):Depth 100-200	4.97824	6.06427	56.16	0.000000	***
	s(day.of.year):Depth >200	5.82775	6.97532	52.20	0.000000	***
	s(day.19840301):Depth 0-5	1.02595	1.05134	0.70	0.405766	
	s(day.19840301):Depth 5-50	1.00000	1.00000	51.99	0.000000	***
	s(day.19840301):Depth 50-100	7.35047	8.26226	11.47	0.000000	***
	s(day.19840301):Depth 100-200	7.51482	8.38288	10.66	0.000000	***
	s(day.19840301):Depth >200	7.70903	8.51629	11.55	0.000000	***

Adjusted R-squared: 0.638, N: 9979, Significance codes: '***' = <0.001, '**' = <0.01, '*' = <0.05

Seasonal Variations

Figure 9 shows the seasonal variations of reflectivity with water depth intervals by color band. All bands have maximum intensities on March 1 and lower local maximums on November 30. The seasonality associated with the blue and green bands, however, differ markedly from the red band in two ways. First, both the intensities of the blue and green bands show minimums in mid-to-late June and maximums in late August, with secondary local minimums in late October. In contrast, the red band shows a monotonic decrease from March 1 to late August. Second, the intensities of the blue and green bands vary distinctly between shallow (<50 ft) and deep ($ $50 ft) water depths, while there is little within-band seasonal variations within the red band. Within the blue and green bands, the amplitudes of seasonal variations are greater at deeper water depths. In addition, the seasonal variations in the deep and shallow water are also approximately in phase in the blue band intensities, but peaks and troughs at shallow depths generally precede those at deeper depths in the green band.

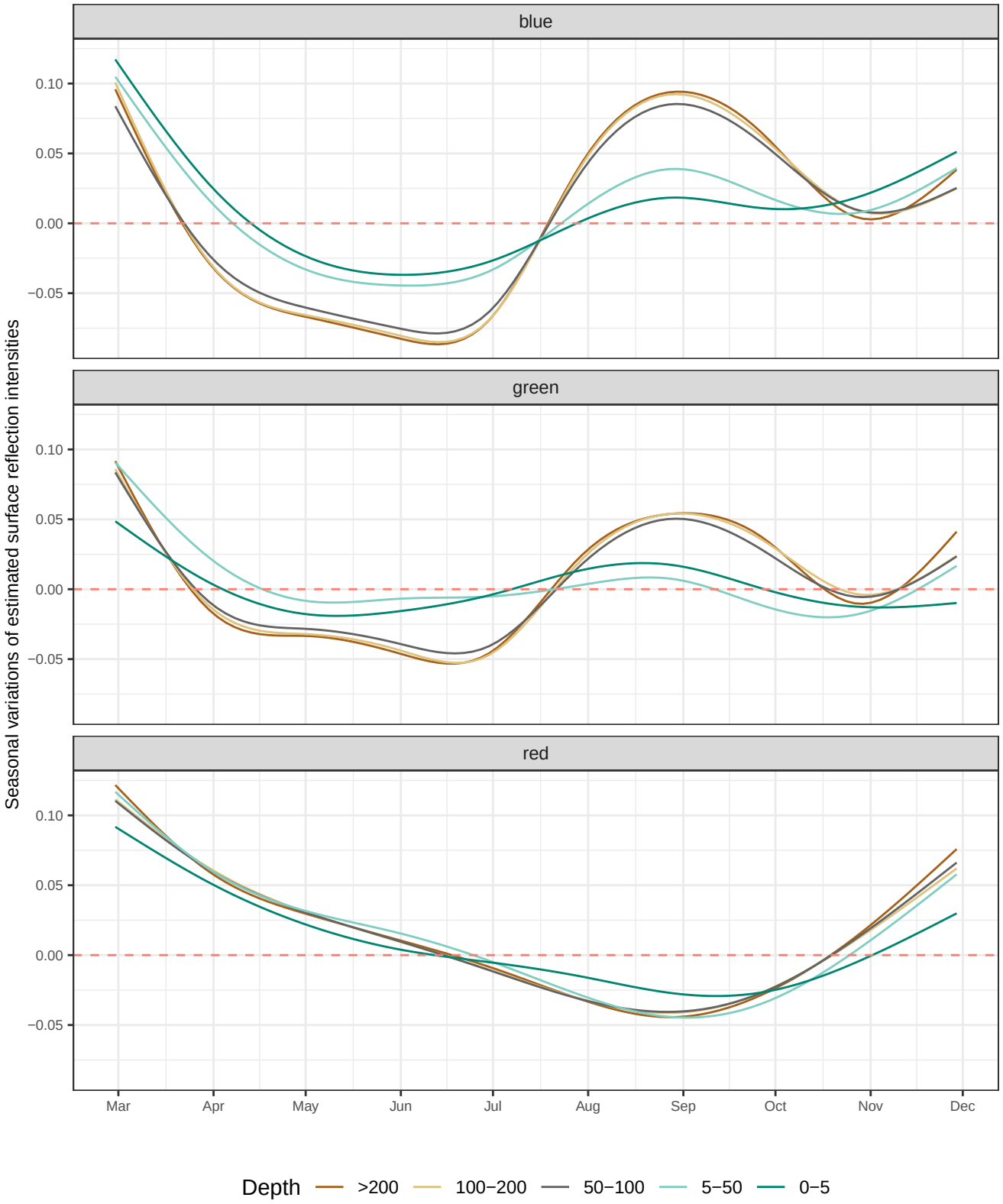

Figure 9. Seasonal variations of estimated surface reflection intensities of blue, green, and red light from Torch Lake in Antrim County, Michigan

Figure 10 shows the seasonal variations in surface reflectance of visible light based on the generalized additive models of blue, green, and red bands for Torch Lake, Michigan. Although the images are not true color, their hues vary from turquoise to Cerulean Blue, while the tones varies seasonally with achromatic shades of grey corresponding to the light intensity from all three color bands (eqn. 9) reaching a a peak in mid-summer and at the beginning and ending of the open-water period.

$$|\ {}_{(c)}\hat{\ddot{\mathcal{R}}}\ | = \sqrt{{}_{(c)}\hat{\ddot{\mathcal{R}}}^2_{blue} + {}_{(c)}\hat{\ddot{\mathcal{R}}}^2_{green} + {}_{(c)}\hat{\ddot{\mathcal{R}}}^2_{red}} \tag{9}$$

where: (c) is the component for seasonality (s) or trend (t) of the predicted value. When components are predicted, all other terms in the GAM prediction are set to their reference levels of zero. In this report, this includes the GAM intercept plus the seasonal or trend component (deviance).

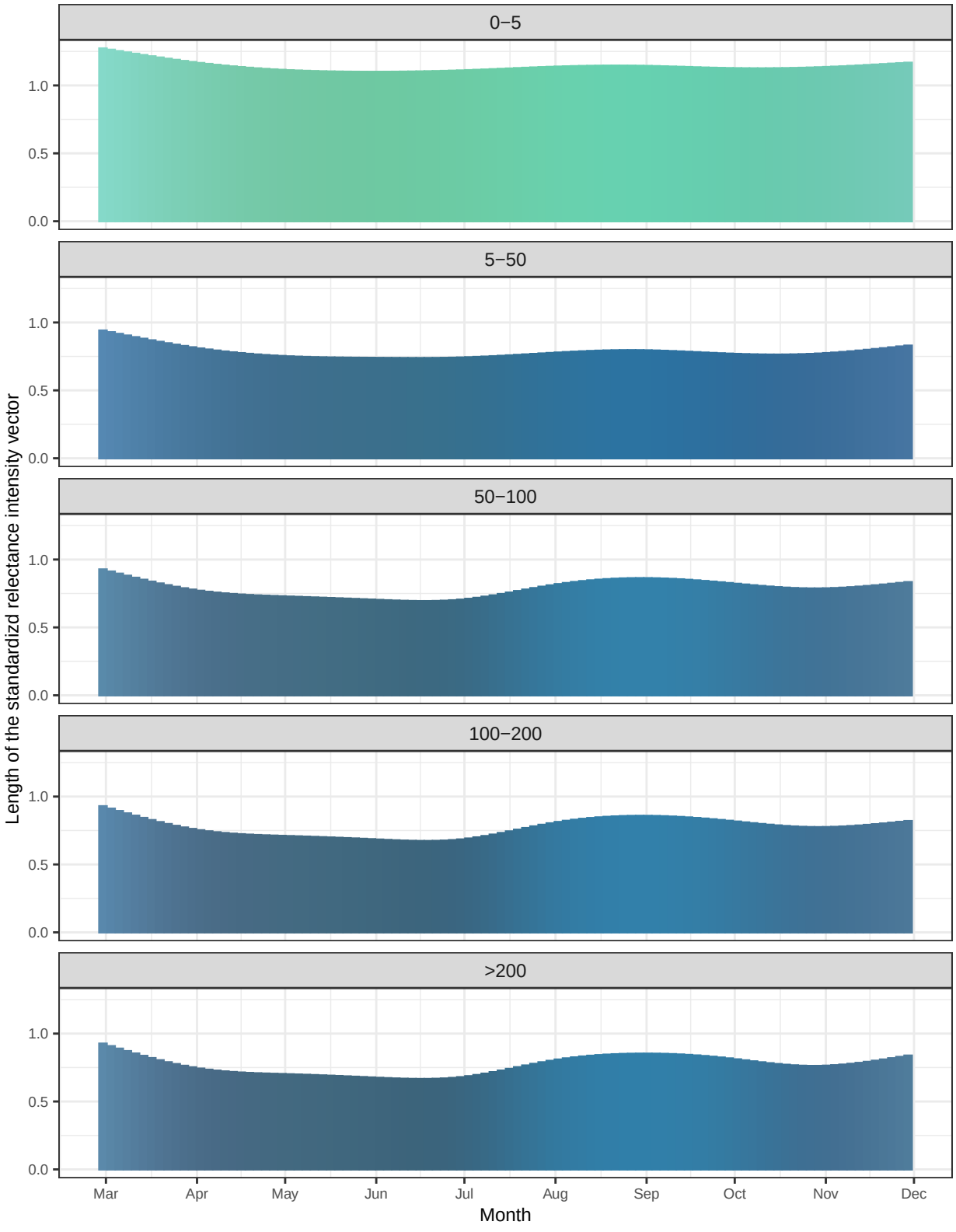

Figure 10. Reconstructed seasonal variations in visible light reflectance from Torch Lake estimated using Landsat 5 parameters data from blue, green, and red bands from 1984-2023 by water-depth interval

Local Levels and Trends

Figure 11 shows the local level components of surface reflectance by water-depth intervals for visible light in the blue, green, and red bands. Intensities for all bands and water depths begin the period of record with positive deviances and end the period with negative deviances. Like seasonality, there is little within-depth variability of intensities for deeper ($\geq$ 50 ft) water depths. For the blue and green bands, intensities at shallower depths (<50 ft) are initially less than those at the three deeper water depths, with the 0-5 ft depth having substantially lower intensities than the 5-50 ft depths. For the blue and green bands, the intensities of both the shallower depths increase above the deeper depths during the middle of the period of the study. Reflectance intensities at all depths then undulate together until decreasing below 0 deviance after 2011. For the red band, the deeper ($ $50-ft) water depths decrease with small sinusoidal oscillations during the period of record, while decreases at the two shallower water-depths are approximately linear.

The onset and proliferation of golden-brown algae would likely be most evident in the reflectances at the shallowest water depth (0-5 ft) because the overlying water column would be at a minimum. Up until the late 1990s, the intensities of green light reflectances at the shallowest depths were generally negative, while reflectances in deeper waters were positive. There is evidence of a transition from the late 1990s to the about 2010 when green reflectances were positive at all water depths. After that, the intensities of green reflectances at deeper water depths continued to decrease relative to the reflectances at the shallowest depth. So, the relative change in reflection intensities of green light between shallow and deeper water depths over time may be the most sensitive indicator of the presence of golden-brown algae attributable to this study of reflectances.

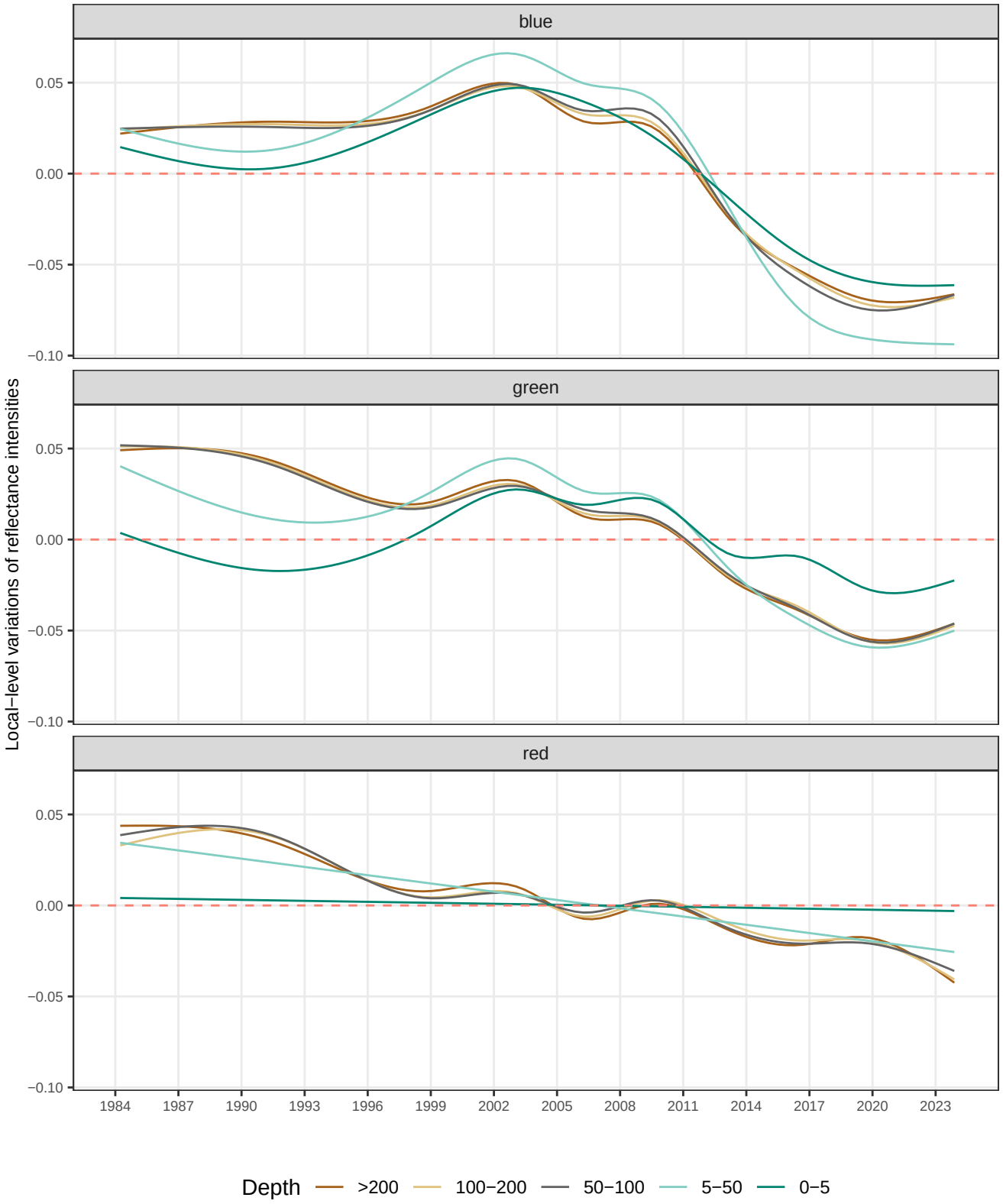

Figure 11. Local level variations in reflectances of blue, green, and red light during open-water periods from 1984 through 2023 on Torch Lake in Antrim County, Michigan

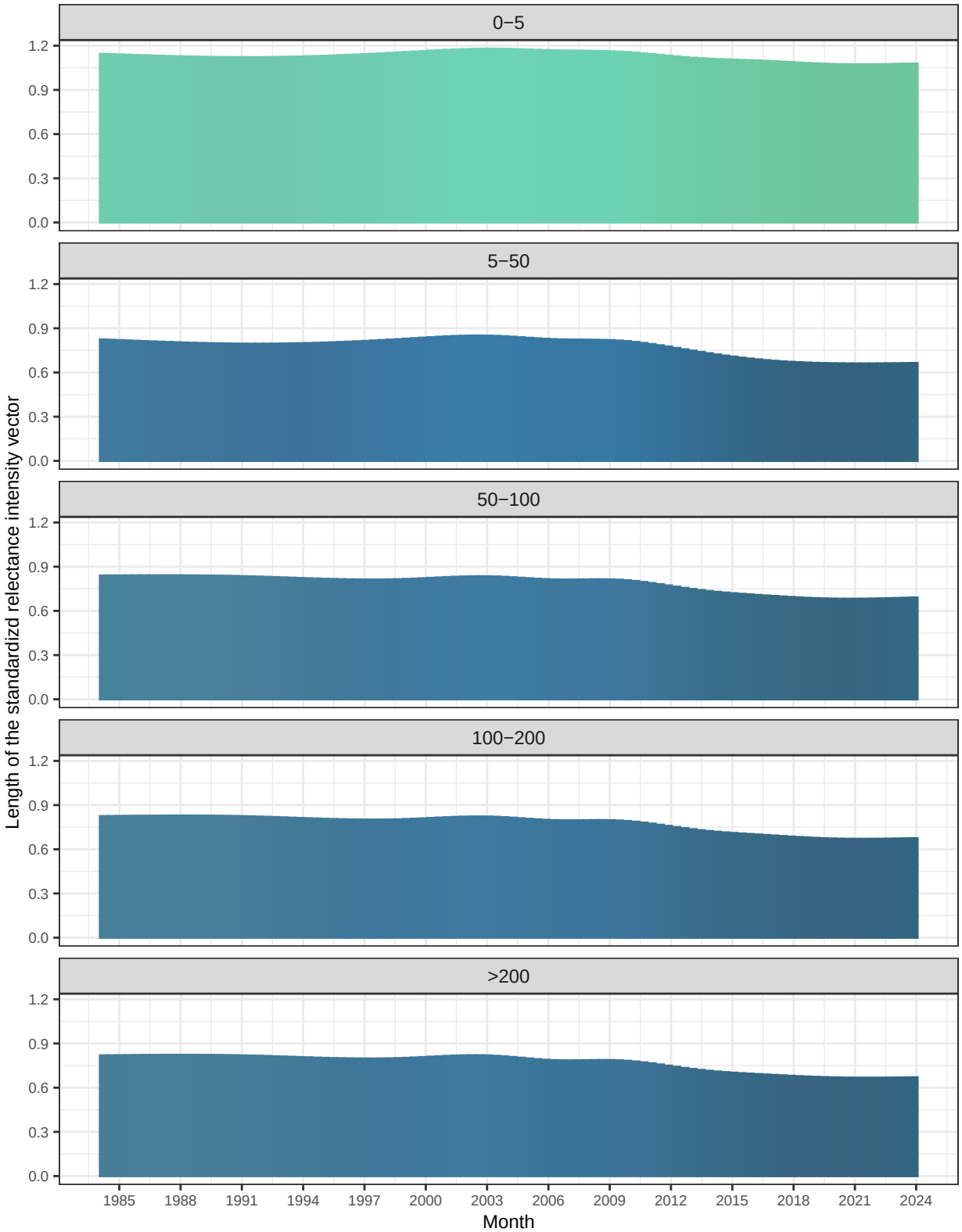

Figure 12. Reconstructed local level variations in visible light reflectance from Torch Lake estimated using Landsat data from blue, green, and red bands from 1984-2023 by water-depth interval

Grand Traverse Bay

Distribution Analysis

Two regions of interest regions of interest were defined in the East and West Arms of Grand Traverse Bay (GTB) based on the 100-m depth contour (fig. 1). Both regions are comparable in size, shape, orientation, and latitudinal span as Torch Lake, although the West Arm has a smaller surface area than the East Arm. There were 830 satellite images from the East Arm of GTB and 653 images from the West Arm of GTB in the dataset obtained from the GEE analysis for blue, green, and red bands of visible light.

Although the nominal range of $\mathcal{R}$ is from 7,273-43,636, the empirical range of the medians is generally contained within the interval from 7,100 to 13,200 (fig. 13.) The East and West Arms had similar empirical cumulative probability distributions with red band values consistently lower than (shifted left from) the green and blue band values. Within this range, there is some positive (right) skewness of about 1.6 to 2.3). In the East and West Arms of GTB, the range defined by these limits contains about 98 percent of the median values for all bands. Finally, values in the truncated SR distribution were rescaled by subtracting the lower empirical limit (eqn. 2) to form the rescaled SR values $\mathring{\mathcal{R}}$.

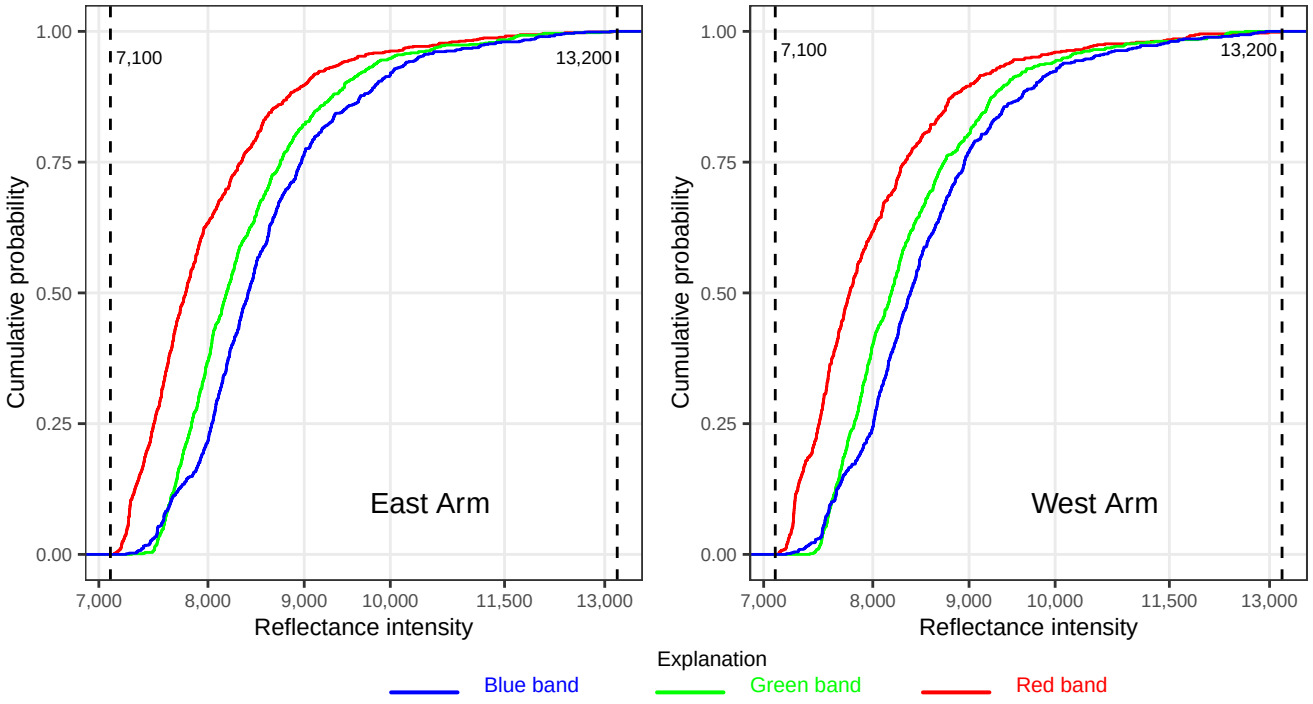

Figure 13. Cumulative probabilities of blue, green, and red bands of surface reflectance intensities for water depths greater than 100 meters in the East and West Arms of Grand Traverse Bay, Michigan

Figure 14 shows rescaled ($\mathring{R}$) and transformed ($\dot{R}$) surface reflectances from the East and West Arms of Grand Traverse Bay. Only one depth interval of greater or equal to 100 m was used in the analysis. Thus, the same γ values of [0.450, 0.540, 0.590] used for the deeper water-depth intervals were used for reflectances from the blue, green, and red bands were used, respectively (table 6). Like the reflectance distributions for Torch Lake, the transformed reflectances for Grand Traverse Bay were shifted to the right and more symmetrical than the rescaled values. Also, the transformed reflectances for the East and West Arms had a similarly shaped probability density function.

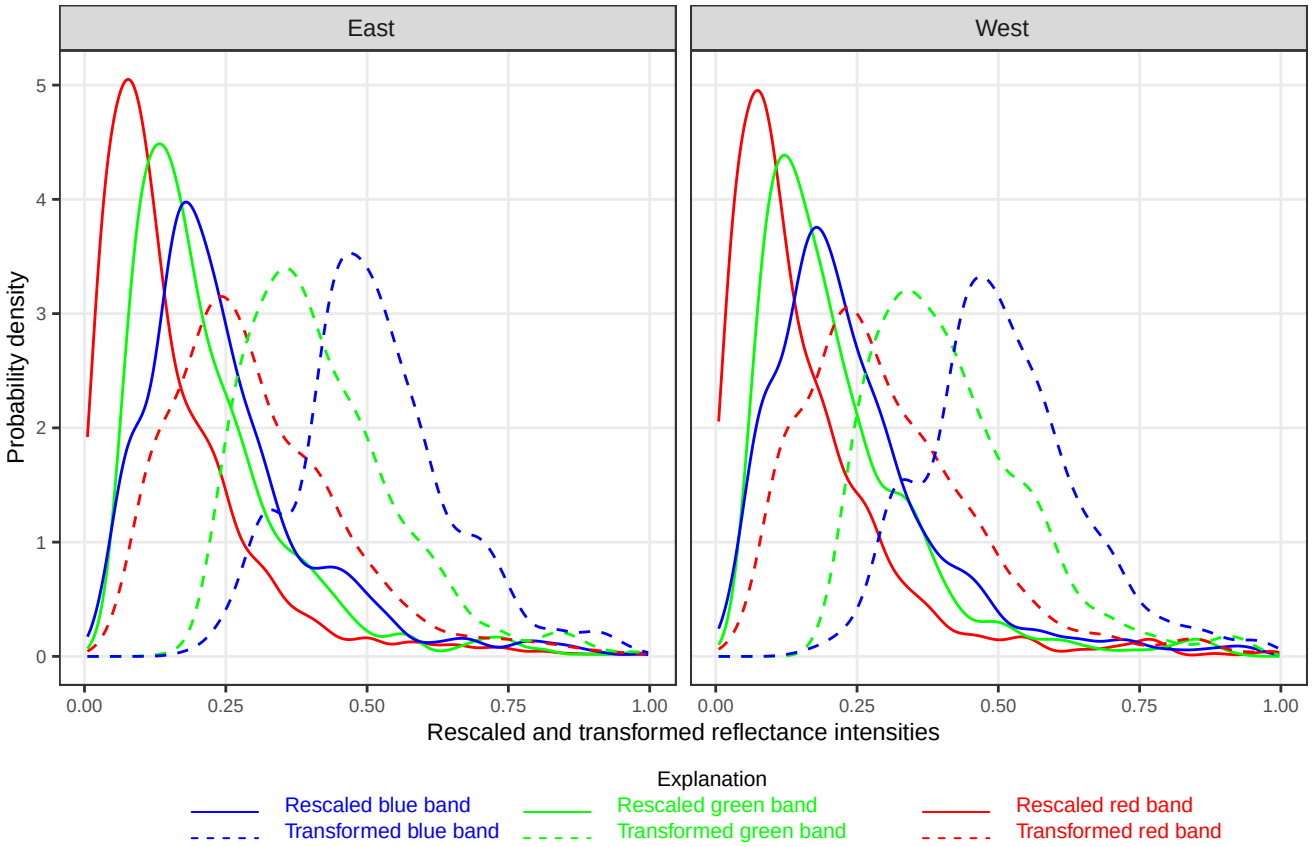

Figure 14. Probability densities of rescaled and transformed blue, green, and red bands of surface reflectance intensities for water depths greater than 100 meters in the East and West Arms of Grand Traverse Bay, Michigan

Atmospheric Adjustment

Katsaros et al. (1985) indicated that the albedo for cloudy skies may be greater than the albedo for clear skies due to reflections back from the water surface from the undersides of clouds. To investigate this possibility with the $\dot{\mathcal{R}}$ data, cloudiness was indexed by an inverse relation percentage of pixels measured after eliminating pixels indicated as clouds, cloud shadows, or ice by the *QA_PIXEL* band.

Parameters for the atmospheric bias adjustment monotonically decreasing equation 5 were estimated using the blue, green, and red $\dot{\mathcal{R}}$ values for ROI in the East and West arms of Grand Traverse Bay. The estimated a and b parameters for the decay function are listed in table 11. Both parameters were highly significant (p-value < 0.001) for all bands and arms. The downward trend in the decay function is thought to be associated with atmospheric effects in which increasing numbers of observed pixels may be associated with clearer skies and reduced re-reflection of light from the undersides of clouds. The a parameters in the East Arm had lower magnitudes and standard errors than the corresponding bands in the West Arm. The b parameter magnitudes in the East Arm were lower than the West Arm for corresponding bands, but the standard error had similar magnitudes. The ROI for the East Arm is larger than the West Arm that may help explain the subsequently greater probabilities of at least one measured pixel to define the median surface reflectances for each satellite pass. Figures 15 and 16 show the decay functions and transformed $\dot{\mathcal{R}}$ and bias-adjusted reflectances $\ddot{\mathcal{R}}$, respectively.

Table 11. Parameters of nonlinear decay function for Grand Traverse Bay

		Parameters for nonlinear model:					
		East Basin			West Basin		
Parameter	Statistic	Blue	Green	Red	Blue	Green	Red
a	estimate	0.5989***	0.4999***	0.3940***	0.648***	0.57***	0.490***
	std.error	(0.0082)	(0.0083)	(0.0097)	(0.011)	(0.01)	(0.012)
b	estimate	0.00278***	0.00318***	0.00480***	0.00376***	0.00476***	0.00765***
	std.error	(0.00022)	(0.00027)	(0.00043)	(0.00024)	(0.00028)	(0.00042)
N		799	804	800	626	632	630
predict	100-%	0.4535	0.3638	0.2437	0.4452	0.3516	0.2280
bias	adjustment	0.1365	0.1262	0.1463	0.1948	0.2084	0.2520

*** indicates p-value < 0.001

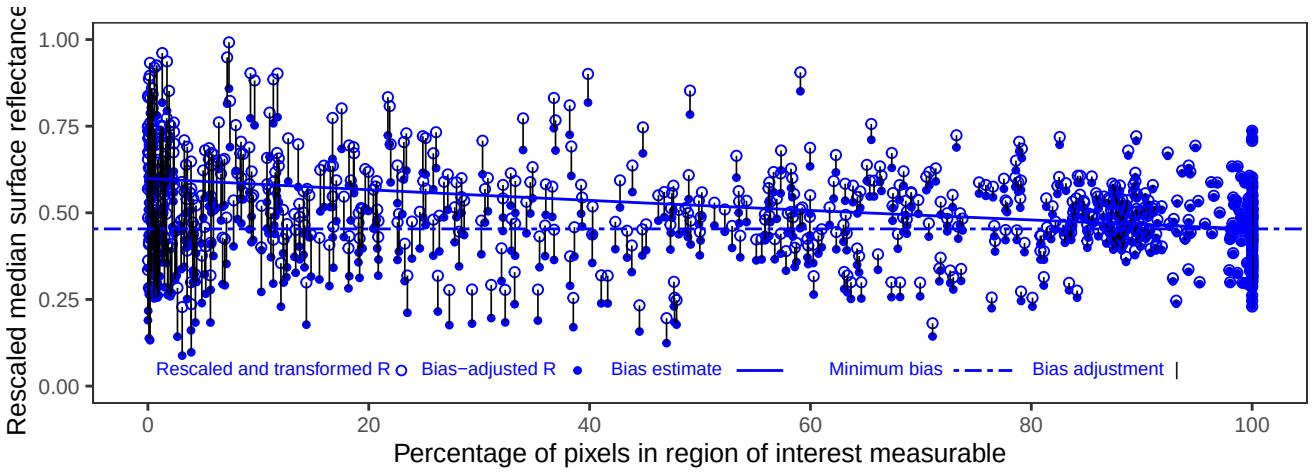

(a) Blue band

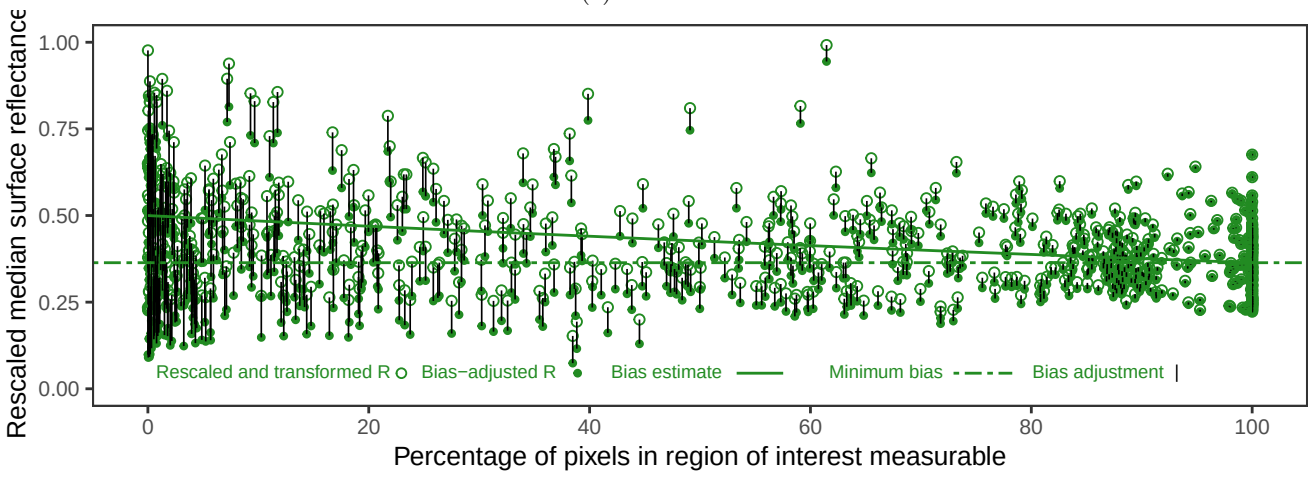

(b) Green band

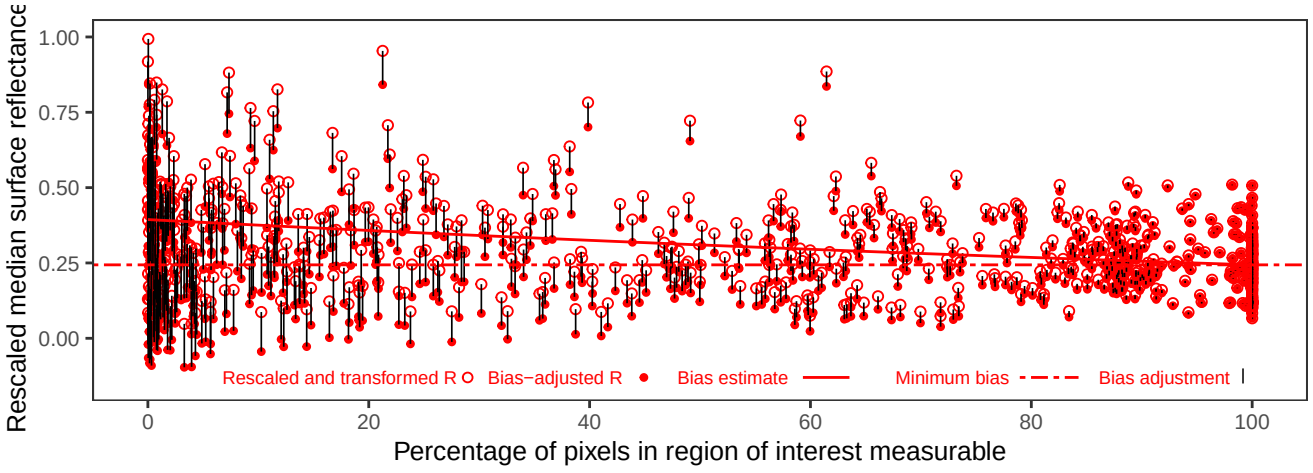

(c) Red band

Figure 15. Rescaled blue, green, and red median surface reflectances from the East Arm of Grand Traverse Bay

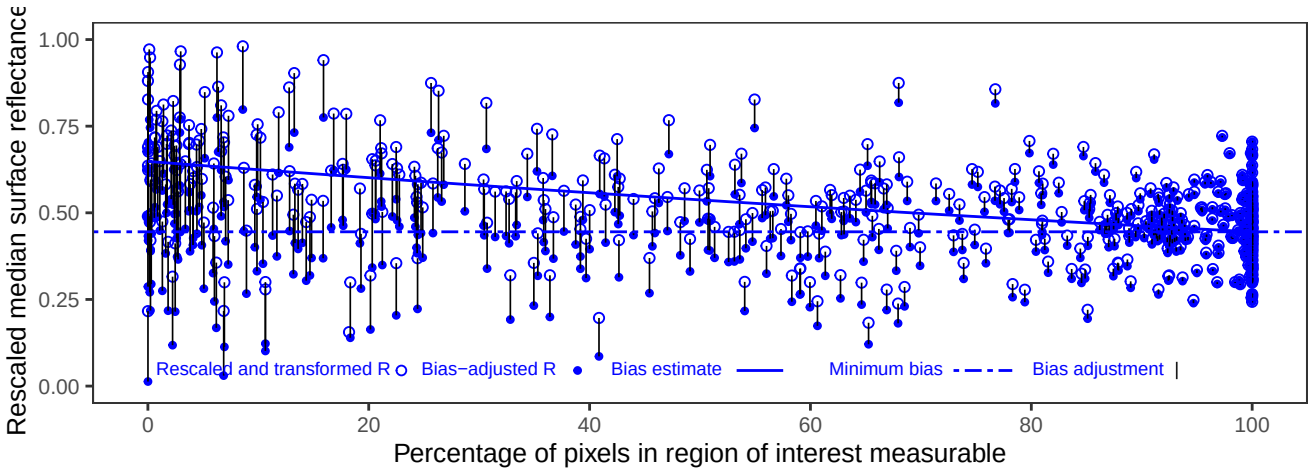

(a) Blue band

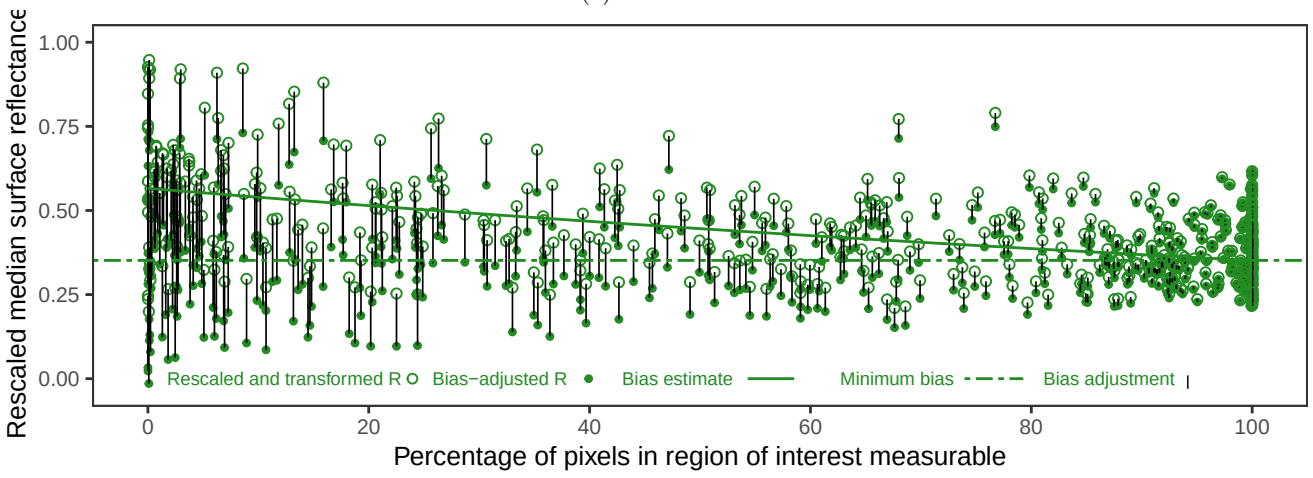

(b) Green band

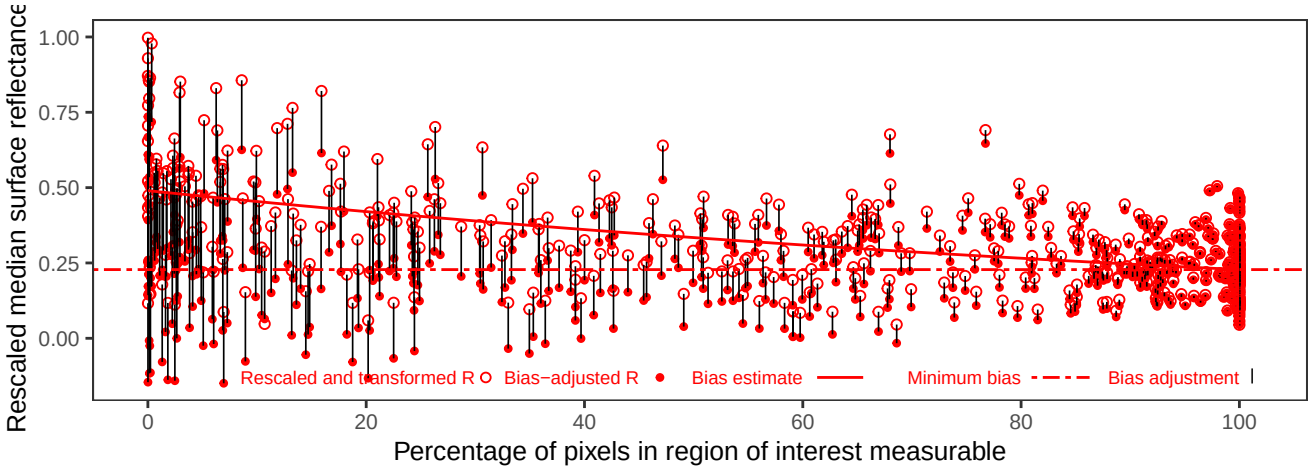

(c) Red band

Figure 16. Rescaled blue, green, and red surface median surface reflectances in the West Arm of Grand Traverse Bay

Generalized Additive Modelling

Table 12 provides summary statistics for GAMs of $\ddot{\mathcal{R}}$ developed using blue, green, and red bands of Landsat data for two regions of interest in Grand Traverse Bay. All bands contain the same components, including parametric terms for an intercept, and factor variables for Satellites `SAT` and east and west arms `Arm` of GTB. Smooth terms include season `s(day.of.year)` and local level `s(day.19840301)`. Explanatory terms are generally highly significant (p-value < 0.001) for all bands, except for the factor variable `Arm` that distinguishes the east and west arms of GTB (p-values > 0.05). The adjusted r-squared values for reflectances in the blue, green, and red bands are 0.561, 0.436, and 0.418, respectively, which indicates a weak to moderately strong relation between $\ddot{\mathcal{R}}$ and the included parametric and smooth terms.

For the parametric terms, the signs of the factor variables for satellites are negative indicating that the reflectances are, on average, lower for Landsat satellites LE07, LC08, and LC09, than for LT05. Parameters for satellites LC08 and LC09 are lower than the negative values for LT07. The factor variable Arm of GTB is not generally statistically significant. The smooth terms for season `s(day.of.year)` and local level `s(day.19840301)` are significant for all bands. Seasonality may account for more variability than the local level as indicated by larger F-values for the seasonal term.

Figures 17 and 18 show the seasonality and local levels detected in surface relectances for GTB. Season reflectance generally peaks in March and declines rapidly though early April. Then, reflectances generally decrease more slowly, becoming negative in July and continuing to decrease through mid-September. In late September, reflectance increase to near March levels. The blue band shows the greatest seasonal variation.

local levels in surface reflectance generally decrease from 1984 through 2023. In 1984, green, blue, and red band surface reflectances have positive deviances of about 577, 386, and 276, respectively. By the end of 2023, the corresponding bands converge to negative deviances of -169, -150, and -150, with no apparent significant differences between bands.

Table 12. Results of Generalized Additive Modeling for surface reflectances of Grand Traverse Bay in Michigan

(a) Blue band

Component	Term	Estimate	Std Error	t-value	p-value	
A. parametric coefficients	(Intercept)	0.4808	0.0044	109.390	0.000000	***
	SAT LE07	-0.0014	0.0059	-0.237	0.812330	
	SAT LC08	-0.1540	0.0087	-17.613	0.000000	***
	SAT LC09	-0.1537	0.0144	-10.708	0.000000	***
	Arm West	-0.0033	0.0038	-0.863	0.388397	
Component	**Term**					
B. smooth terms	s(day.of.year)	7.7941	8.6221	28.485	0.000000	***
	s(day.19840301)	5.7844	6.8639	16.746	0.000000	***

Adjusted R-squared: 0.561, N: 1425, Signif. codes: '***' = <0.001, '**' = <0.01, '*' = <0.05

(b) Green band

Component	Term	Estimate	Std Error	t-value	p-value	
A. parametric coefficients	(Intercept)	0.3898	0.0048	81.659	0.000000	***
	SAT LE07	-0.0231	0.0064	-3.589	0.000344	***
	SAT LC08	-0.1046	0.0095	-11.048	0.000000	***
	SAT LC09	-0.0872	0.0155	-5.635	0.000000	***
	Arm West	-0.0078	0.0041	-1.882	0.060065	.
Component	**Term**					
B. smooth terms	s(day.of.year)	7.4868	8.4297	22.393	0.000000	***
	s(day.19840301)	5.7035	6.7807	22.937	0.000000	***

Adjusted R-squared: 0.436, N: 1436, Signif. codes: '***' = <0.001, '**' = <0.01, '*' = <0.05

(c) Red band

Component	Term	Estimate	Std Error	t-value	p-value	
A. parametric coefficients	(Intercept)	0.2745	0.0053	52.053	0.000000	***
	SAT LE07	-0.0243	0.0071	-3.400	0.000693	***
	SAT LC08	-0.1273	0.0105	-12.107	0.000000	***
	SAT LC09	-0.1052	0.0173	-6.095	0.000000	***
	Arm West	-0.0111	0.0046	-2.399	0.016564	*
Component	**Term**					
B. smooth terms	s(day.of.year)	6.0190	7.1786	37.374	0.000000	***
	s(day.19840301)	4.9494	5.9883	9.539	0.000000	***

Adjusted R-squared: 0.418, N: 1430, Signif. codes: '***' = <0.001, '**' = <0.01, '*' = <0.05

Seasonal Variations

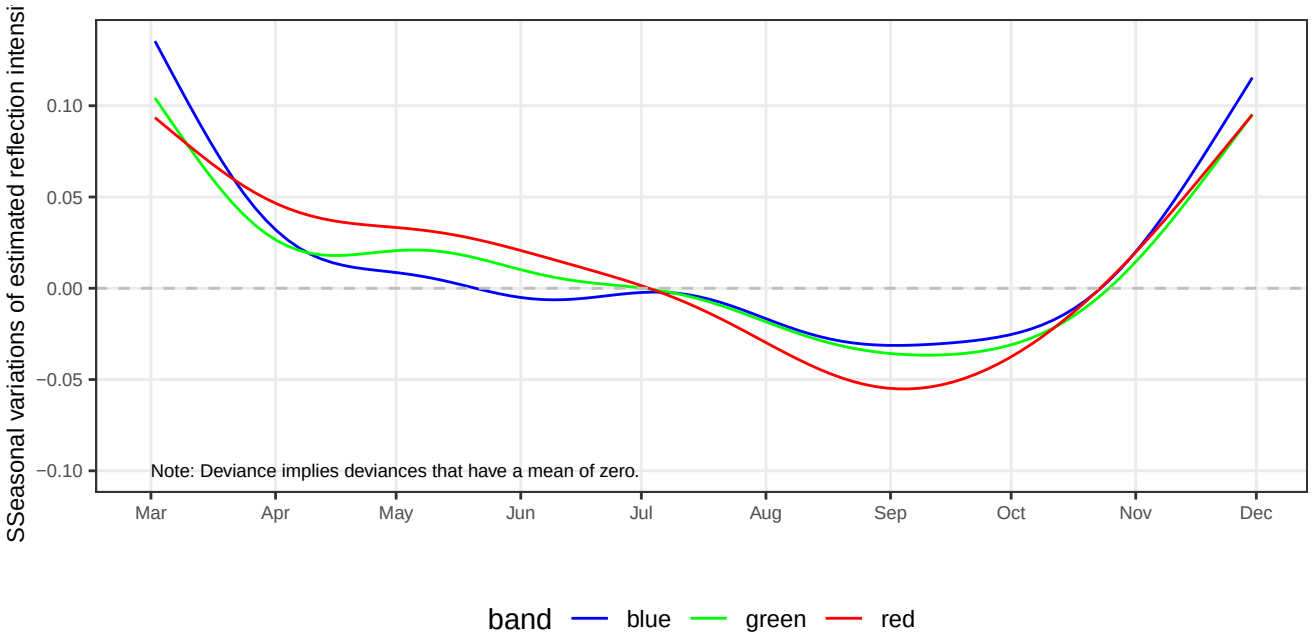

Figure 17. Seasonal variations of reflection intensities from Grand Traverse Bay, Michigan

Local Levels and Trends

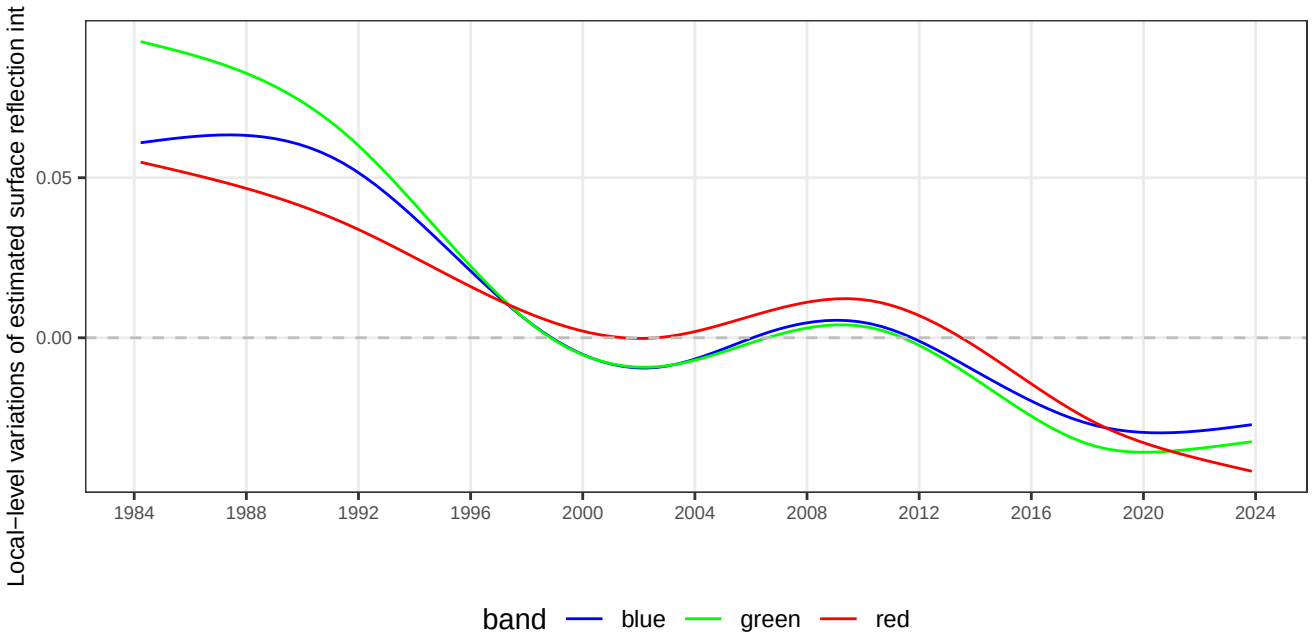

Figure 18. Local-level variations of surface reflectance intensities from Grand Traverse Bay, Michigan

Discussion

This report describes an analysis of Landsat surface reflectance imagery in the blue, green, and red frequency bands of visible light form Torch Lake. Much of the focus of the report is on identifying seasonality and trends interpreted from smooth components of blue, green, and red bands. The seasonality and trend components were compared and contrasted with those determined for selected regions of interest in Grand Traverse Bay.

(Rocchio, Laura E.P. 2023) noted that data from Landsat 5 and 7 may overestimate reflectance from aquatic surfaces by more than 25 percent, resulting in a false downward trend when combined with data from Landsat 8 and 9. To mitigate this concern, a factor satellite variable `SAT` was used to account for different mean sensitivities to reflectance intensities for each satellite. Table 13 provides a percent bias reduction for each band and satellite, computed by dividing the satellite level parameter by the GAM model intercept. Without harmonizing the satellite data, these differences could have created biases in trend consistent with those indicated by Rocchio (2023).

Table 13. Bias reductions associated with incluing the factor variable SAT in estimation of surface reflections from Torch Lake, Michigan

[!h]

Satellite ID	band	Model intercept	Satellite level parameter	Bias reduction (percent)
LE07	blue	0.52630	-0.03515	-6.68
LC08	blue	0.52630	-0.14645	-27.83
LC09	blue	0.52630	-0.15398	-29.26
LE07	green	0.67356	-0.04746	-7.05
LC08	green	0.67356	-0.09059	-13.45
LC09	green	0.67356	-0.05379	-7.99
LE07	red	0.29371	-0.04469	-15.21
LC08	red	0.29371	-0.10350	-35.24
LC09	red	0.29371	-0.09129	-31.08

(Maciel et al. 2023) also noted that aquatic reflectances likely have different atmospheric corrections than surface reflectance data from land surfaces. To mitigate this concern, an adjustment for atmospheric effects was estimated by use of decay functions. These functions related the percent of measurable pixels in an aquatic region of interest obtained from a particular scene to the maximum number of pixels measured under cloudless conditions. These functions were used to reduce the bias of surface reflectances from blue, green, and red frequency bands from Torch Lake and Grand Traverse Bay.

Generalized Additive Models (GAM) with similar components were estimated for reflectances from blue, green, and red visible light from both Torch Lake and selected regions of interest in Grand Traverse Bay. Torch Lake was stratified by five water depths from shallow to deep, whereas, the regions of interest in Grand Traverse Bay only included water depths greater than 100 m. The shallower areas included in the Torch Lake analysis likely included reflectances from the water column and the lakebed, including reflectances from any benthic algae communities, while deeper areas in Torch Lake and those from Grand Traverse Bay only reflected those from the water column. Thus, inclusion of shallow water depths in the Torch Lake analysis likely increased the variability of reflectance intensities relative to those of Grand Traverse Bay. Much of this variability in the Torch Lake data was explained by the factor variable *Depth*, and contributed to the increased r^2 values for blue, green, and red band reflectances

from 0.740, 0.815, and 0.638 for Torch Lake, as compared with 0.561, 0.436, and 0.418 for Grand Traverse Bay.

The GTB analysis provides a basis to compare and assess estimated seasonality and trends on GTB with those on Torch Lake. The seasonality of bands on GTB (fig. 17) are similar to one another and to the seasonality of the red band on Torch Lake (fig. 9). The blue and green bands on Torch Lake (also fig. 9), however, are dissimilar to the others, especially when attention is focused on the deeper (>50 ft) water depths where the amplitude of seasonal variations are greater. The concordance between the red band on Torch Lake and all bands on GTB confirms some similarities between the two waterbodies. The discordance between the blue and green bands on Torch Lake and corresponding bands on GTB indicates that somewhat different processes may be occurring in Torch Lake.

All linear terms and smooth terms for the seasonal components were statistically significant (p-values less than 0.001) for all frequency bands and all water-depth intervals. Smooth terms for local trend components were also highly significant for all water-depths for the blue and green frequency bands, although some water-depth intervals were not highly significant for the red frequency band. The r-squared values for the GAM models for the blue, green, and red frequency bands were 0.740, 0.815, and 0.638, respectively, indicating moderately strong to strong effect size.

Seasonal variations in frequency bands were similar for all frequency bands on Grand Traverse Bay and for the red band on Torch Lake. Here, the highest reflectances occurred on March 1, and then declined monotonically until early September, when seasonal reflectances started to increase until November 30. Differences between seasonal reflectances for Grand Traverse Bay showed little apparent differences among frequency bands, nor did seasonal frequencies for the red band show substantial differences among water-depth intervals for Torch Lake. In contrast, seasonal frequencies for blue and green band frequencies on Torch Lake showed a secondary peak in early September, with subsequent decreases in reflectances until late October, which was followed by a rise until November 30. Also, the amplitude of seasonal reflectances increased markedly with increased water-depth interval on Torch Lake, particularly in the blue band frequency.

The causes of these differences in seasonal reflectances are not well understood. For the blue band frequencies, the lower amplitudes of seasonal reflectivities in the two shallower water-depth intervals (0 to 5-ft and 5 to 50-ft) in Torch Lake may be attributed to a combined effect of water and lake-bottom reflectances. For the three deeper intervals (>50 ft), the seasonal reflectances are similar in the blue band frequencies and likely do not include lake-bottom reflectances. The seasonal reflectances may be helpful, however, in determining the timing of future field water-quality profiling and sampling. In particular, spectrophotometer profiling in mid June, near September 1, and again in mid-October may be helpful in confirming the surface reflectance characteristics obtained from Landsat satellites, especially in the deeper water-depth intervals. In additions, sampling of suspended particulate and algae populations may help better understand the increased reflectance of blue and green light reflectances near September 1.

The local trends estimated in reflectances of blue and green light frequencies are generally similar (fig. 11). Both blue and green frequency reflectances were relatively low beginning in 1984 and generally peaked between 2002 and 2003. Since 2003, reflectances have generally decreased together, although the relatively shallow depth interval from 5 to 50-ft has decreased below 1984 levels. There is also evidence to indicate that higher amplitude fluctuations in the green frequencies are occurred at the shallowest water-depth interval from 0 to 5-ft, during the early period from 1984 to about 2009. Since 2010, the differences in reflectance amplitudes between water-depth intervals seems to have decreased, although the reflectance of the green frequencies in the 0 to 5-ft water-depth interval has not returned to its 1984 level. Reflectances in the shallower water-depth intervals are more likely to be associated where reflectances from benthic algae than reflectances in deeper intervals.

Figure 9 shows that red band reflectance generally decreases from March 1 to mid-September, after which reflectances increase until November 30. The timing of the start of the mid-September increase in red reflectance may be associated with leaf fall and the beginning of seasonal plant decay. Plant decay can release tannins into the water, especially from the leaves of oaks, birches, willows, and pines, as well as some flowering plants (U.S. Forest Service 2024(?)). These tannins can leach into water that drains into streams and lakes, resulting in some brownish coloration, that may be preferentially reflected in the red band. Alternatively, some algae strongly absorb light in the red band, so a drop in reflectance may indicate a growing presence of algae until about September 1. So, water quality sampling for tannins may help resolve this uncertainty. local levels (fig. 11) provide little evidence to support long-term trends in the red band at all water-depth interval.

(Maciel et al. 2023) also noted that aquatic reflectances likely have different atmospheric corrections than surface reflectance data from land surfaces. To mitigate this concern, an adjustment for atmospheric effects was estimated by use of decay functions. These functions related the percent of measurable pixels in an aquatic region of interest obtained from a particular scene to the maximum number of pixels measured under cloudless conditions. These functions were used to reduce the bias of surface reflectances from blue, green, and red frequency bands from Torch Lake and Grand Traverse Bay.

Generalized Additive Models (GAM) with similar components were estimated for reflectances from blue, green, and red visible light from both Torch Lake and selected regions of interest in Grand Traverse Bay. Torch Lake was stratified by five water depths from shallow to deep, whereas, the regions of interest in Grand Traverse Bay only included water depths greater than 100 m. The shallower areas included in the Torch Lake analysis likely included reflectances from the water column and the lakebed, including reflectances from any benthic algae communities, while deeper areas in Torch Lake and those from Grand Traverse Bay only reflected those from the water column. Thus, inclusion of shallow water depths in the Torch Lake analysis likely increased the variability of reflectance intensities relative to those of Grand Traverse Bay. Much of this variability in the Torch Lake data was explained by the factor variable *Depth*, and contributed to the increased r^2 values for blue, green, and red band reflectances from 0.740, 0.815, and 0.638 for Torch Lake, as compared with 0.561, 0.436, and 0.418 for Grand Traverse Bay.

The GTB analysis provides a basis to compare and assess estimated seasonality and trends on GTB with those on Torch Lake. The seasonality of bands on GTB (fig. 17) are similar to one another and to the seasonality of the red band on Torch Lake (fig. 9). The blue and green bands on Torch Lake (also fig. 9), however, are dissimilar to the others, especially when attention is focused on the deeper (>50 ft) water depths where the amplitudes of seasonal variations are greater. The concordance between the red band on Torch Lake and all bands on GTB confirms some similarities between the two waterbodies. The discordance between the blue and green bands on Torch Lake and corresponding bands on GTB indicates that somewhat different processes may be occurring in Torch Lake.

Seasonal variations in frequency bands were similar for all frequency bands on Grand Traverse Bay and for the red band on Torch Lake. Here, the highest reflectances occurred on March 1, and then declined monotonically until early September, when seasonal reflectances started to increase until November 30. Differences between seasonal reflectances for Grand Traverse Bay showed little differences among frequency bands, nor did seasonal frequencies for the red band show substantial differences among water-depth intervals for Torch Lake. In contrast, seasonal frequencies for blue and green band frequencies on Torch Lake showed a secondary peak in early September, with subsequent decreases in reflectances until late October, which was followed by a rise until November 30. Also, the amplitude of seasonal reflectances increased markedly with increased water-depth interval on Torch Lake, particularly in the blue band frequency.

The causes of these differences in seasonal reflectances are not well understood. For the blue band frequencies, the lower amplitudes of seasonal reflectances in the two shallower water-depth intervals (0 to 5-ft and 5 to 50-ft) in

Torch Lake may be attributed to a combined effect of water and lake-bottom reflectances. For the three deeper intervals (>50 ft), the seasonal reflectances are similar in the blue band frequencies and likely do not include lake-bottom reflectances. Sampling of dissolved and suspended materials, including algae populations, may help better understand the changes in seasonal reflectance of blue and green light.

The local levels estimated in reflectances of blue and green light from Torch Lake are generally similar (fig. 11). Both blue and green frequency reflectances were relatively low beginning in 1984 and generally peaked between 2002 and 2003. Since 2003, reflectances have generally decreased together, although the relatively shallow depth interval from 5 to 50-ft has decreased below 1984 levels. There is also evidence to indicate that higher amplitude fluctuations in the green frequencies occurred at the shallowest water-depth interval from 0 to 5-ft, during the early period from 1984 to about 2009. Since 2010, the differences in reflectance amplitudes between water-depth intervals seems to have decreased, although the reflectance of the green frequencies in the 0 to 5-ft water-depth interval has not returned to its 1984 level.

Figure 9 shows that red band reflectance generally decreases from March 1 to mid-September, after which reflectances increase until November 30. The timing of the start of the mid-September increase in red reflectance may be associated with leaf fall and the beginning of seasonal plant decay. Plant decay can release tannins into the water, especially from the leaves of oaks, birches, willows, and pines, as well as some flowering plants (U.S. Forest Service 2024(?)). These tannins can leach into water that drains into streams and lakes, resulting in some brownish coloration, that may be preferentially reflected in the red band. Alternatively, some algae strongly absorb light in the red band, so a drop in reflectance may indicate a growing presence of algae until about September 1. So, water quality sampling for tannins may help resolve this uncertainty. local levels (fig. 11) provide little evidence to support long-term trends in the red band at all water-depth interval.

Violin plots provide a compact depiction of the distribution of a continuous variable that provides more detail on local variations in probability than comparable boxplots. Violin plots of residuals from GAM models shown in tables 8, 9, and 10 are displayed in figure 19. The shapes of these distributions tend to have a similar form across satellites and color bands despite being formed from widely different numbers of observations per satellite. For example, the LT05 distribution is based on an average of 437 images per depth interval, whereas LC09 is based on an average of 17 images (table tbl-SAT_depth_image_counts). Although a somewhat greater range between the minimum and maximum values would be expected with increased sample size taken from the same probability distribution, there is no substantial evidence in the figure to indicate that earlier Landsat satellites (LT05 and LE07) had greater measurement error variance (or lack of precision) than satellites LC08 and LC09. In addition, time series plots of model residuals by satellite and color band showed no evidence of trend or bias (fig. 20), given the factor variable for satellite (SAT) was included in the models.

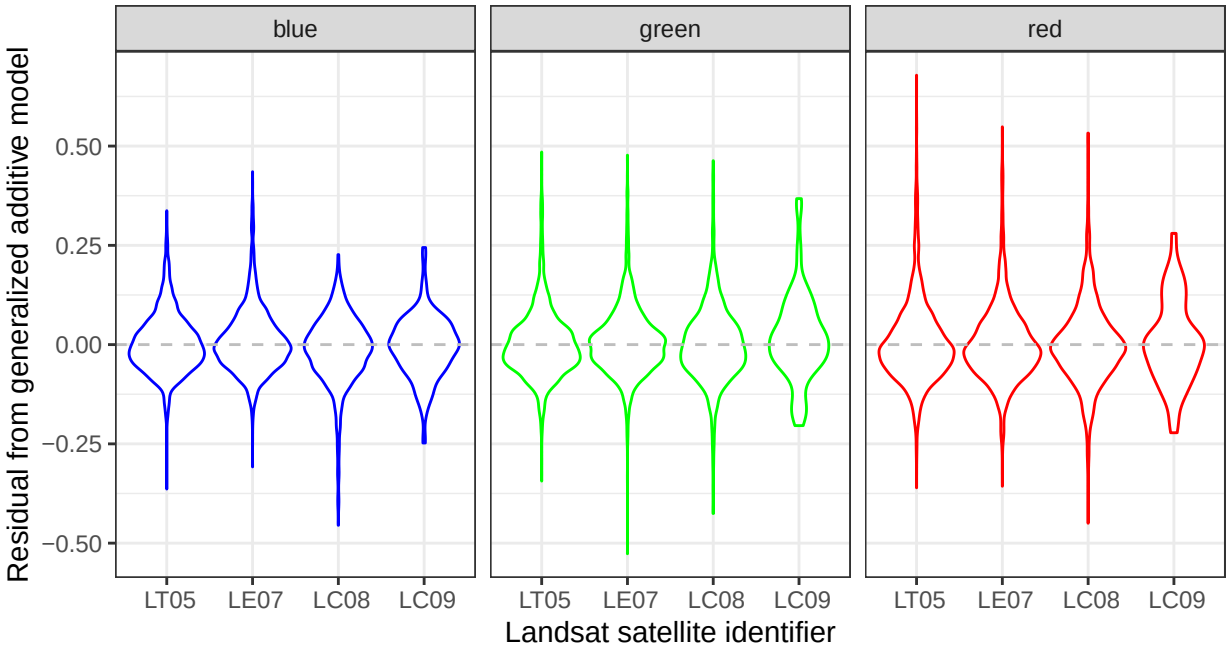

Figure 19. Violin plots of residuals from generalized additive models for estimating rescaled and transformed reflectances by satellite and color band

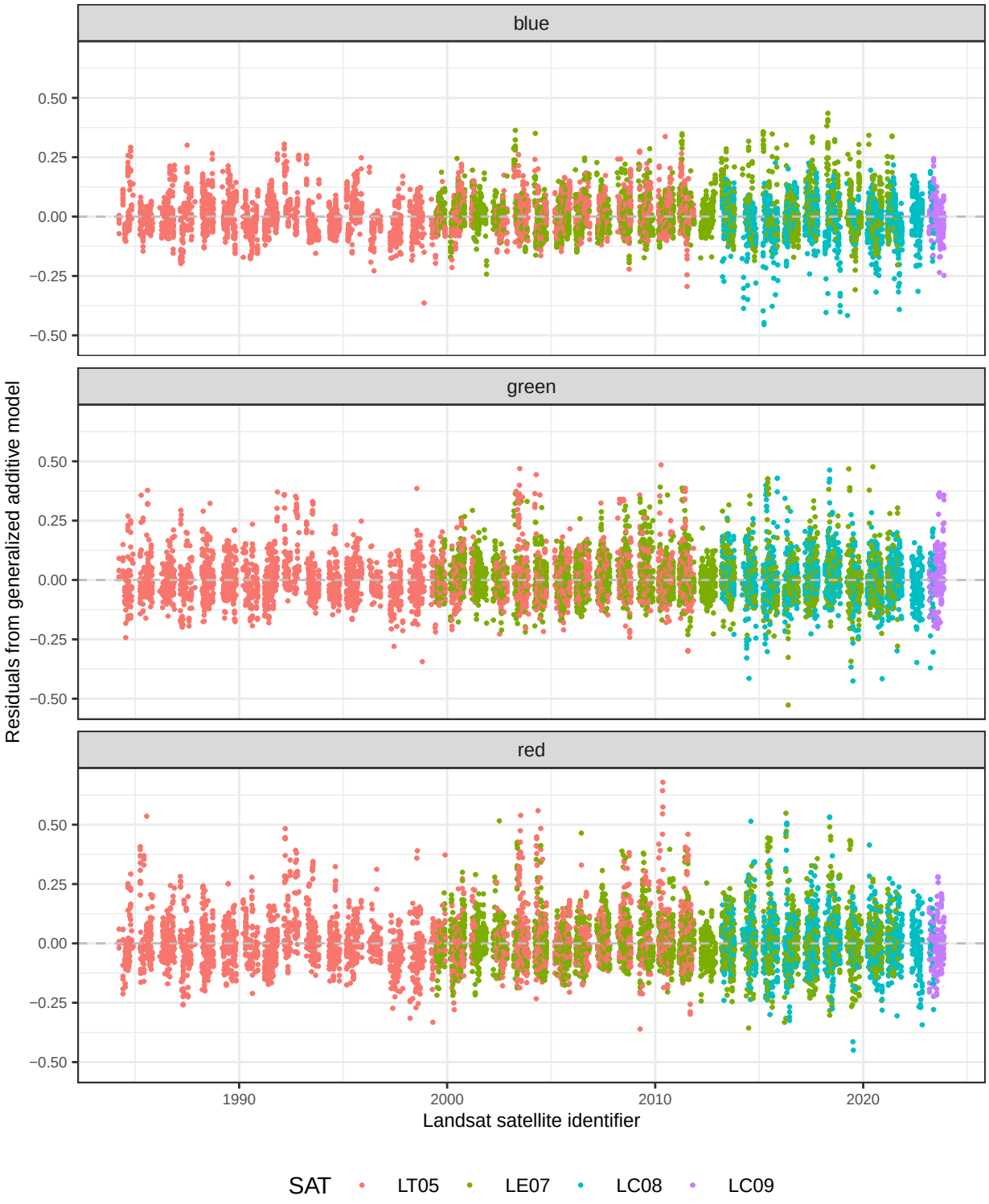

Figure 20. Residual time series of generalized additive models for estimating rescaled and transformed reflectances by satellite

The modelling approach does not account for spatial or temporal correlations in the satellite imagery data, although the assumption of independent identically distributed (i.i.d.) residuals (ϵ_i) underlies the model structure (eqn. 6). Spatial correlation, in particular, is likely to occur because all 10 regions of interest in Torch Lake are imaged at the same time. Thus, the corresponding 10 median measured reflectances for each band are affected by similar atmospheric conditions, causing similar errors (deviations) in reflectances from their true values. This similarity implies a positive spatial correlation structure, which would decrease the effective number of number of measurements and reduce the statistical significance of model parameters as indicated by their reported p-values (tables 8, 9, and 10).

To assess the potential severity of the spatial correlation on model statistics, the model residuals were reorganized to a matrix formed by date (rows) and regions of interest (columns) for all images in which every region of interest had a residual (was successfully measured). Of the 1,129 unique dates of measurements, 873 imaged all 10 regions of interest for all three bands. The correlation matrices computed from the residual matrices are shown on fig. 21. Note that correlations among all regions of interest are numerically positive and blue tinged, based on a color bar from red (-1) to blue (+1). Deeper blues correspond to greater numerical correlations in the lower diagonal of the matrix. The green band (fig. 21 b) appears to have the lowest average off diagonal correlations among regions of interest, corresponding to the model with the highest coefficient of determination (r^2). In any case, all reported p-values are likely to be somewhat higher (have less statistical significance) than indicated in the GAM summary output tables, which were computed under the assumption of residual independence.

Correlations greater than 0.90 are of greater concern. These higher areas tend to be near the main diagonal and clustered within basins at greater water-depth intervals. This implies, for example, that tests of the statistical differences between parameter estimates for 100-200 ft depths versus >200 ft depths in either the north or south basins may be misleading. In particular, the parameter standard errors are likely too small, reflecting the nominal degrees of freedom rather than the effective degrees of freedom, which are reduced by the spatial correlation. Thus, detailed pairwise tests may result in falsely indicating a statistical differences adjacent levels where none exists. Note that the p-values for all factor variables in tables 8, 9, and 10 are based on comparisons with the reference levels rather than and adjacent levels. Generally, the reported p-values are less than 10^{-6}, and the spatial correlation is not likely to change the overall statistical significance of the model or the coefficients of determination.

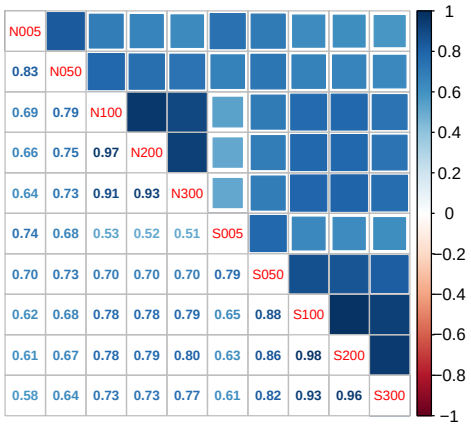

(a) Blue band

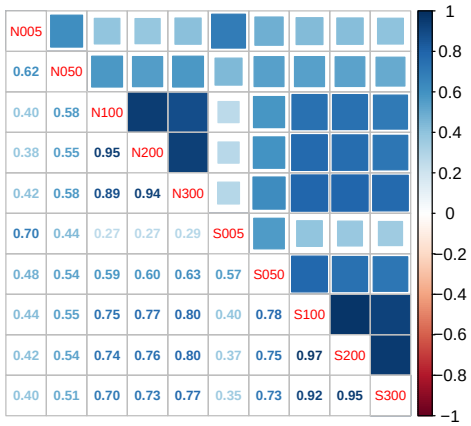

(b) Green band

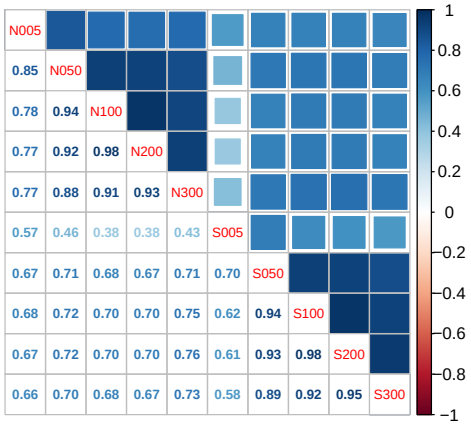

(c) Red band

ROI	Basin	Depth, in feet
N005:	North	0–5
N050:	North	5–50
N100:	North	50–100
N200:	North	100–200
N300:	North	>200
S005:	South	0–5
S050:	South	5–50
S100:	South	50–100
S200:	South	100–200
S300:	South	>200

(d) Explanation

Figure 21. Spatial Correlation of generalized additive modelling errors by basin and water-depth interval for Torch Lake, Michigan

Figure 22 shows the autocorrelation functions of GAM residuals in the blue, green, and red bands by Basin and Depth for Torch Lake. The figure was derived from data provided by Landsat satellites 5, 7, 8, and 9. Each satellite images Torch Lake once every 16 days. The satellite orbits are offset to allow 8-day repeat image with a paired satellite. Shorter than 8-day intervals are available because Landsat 7, 8, and 9 were operating concurrently from 2013 to 2022. The figure shows some positive autocorrelation for separation times of less than 10 days. After 10 days, correlations were both positive and negative, indicating little affect of correlation on the interpretation of model statistics.

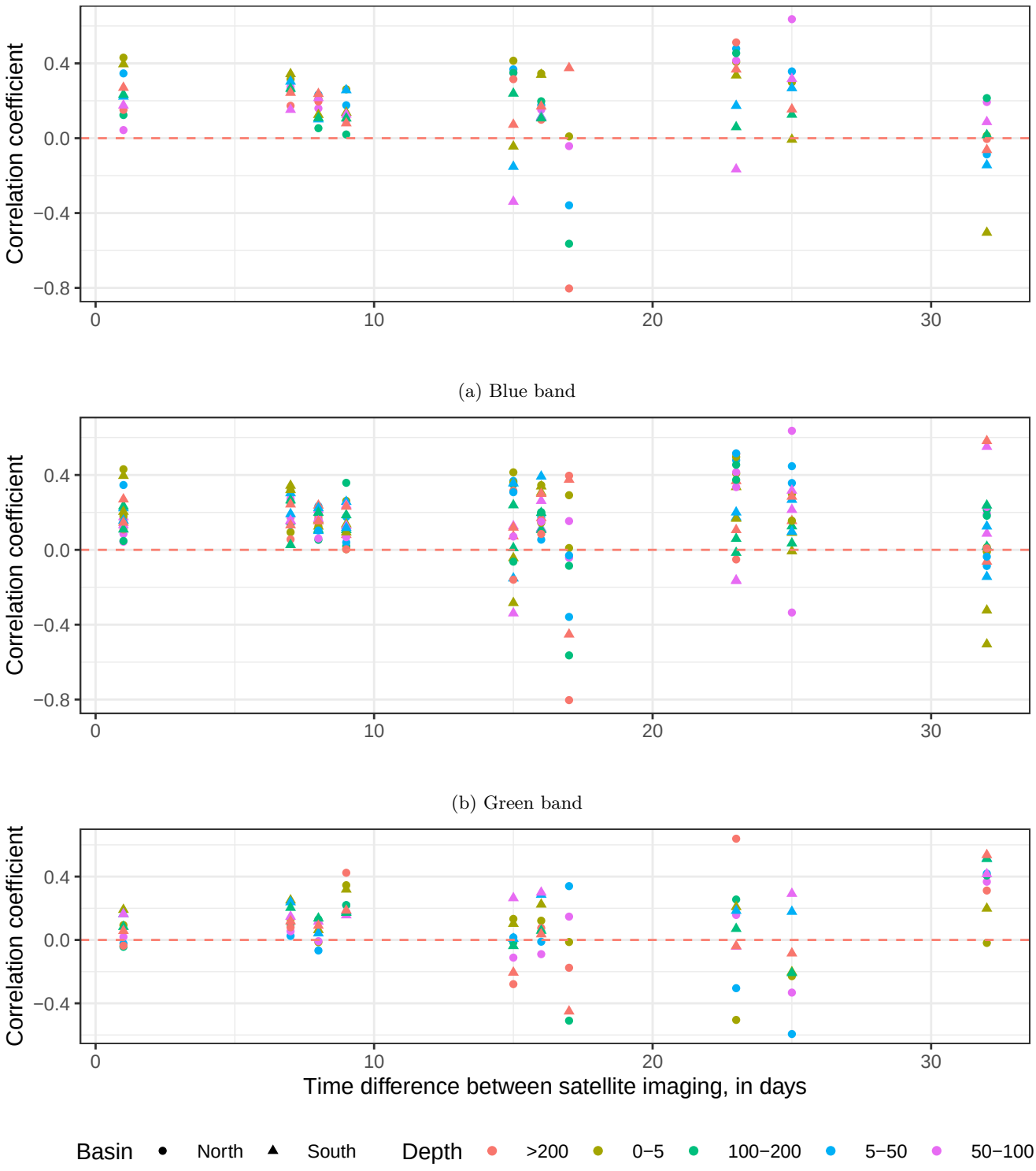

(a) Blue band

(b) Green band

(c) Red band

Figure 22. Autocorrelation functiions of generalized additive modelling errors by basin and water-depth interval for Torch Lake, Michigan

Summary

Landsat satellites, which are jointly managed by NASA and USGS, were analyzed to better understand possible spatial and temporal changes in surface reflectance characteristics of Torch Lake in Antrim County, Michigan. Reflectances in the blue, green, and red bands of visible light from Landsat satellites 5, 7, 8, and 9 were analyzed for generally open-water months from 1984 through 2023. Torch Lake was stratified by five water-depth intervals spanning 0 to >200 ft and by north and south basins. To provide a basis for comparison, two basins were defined in East and West Arms of Grand Traverse Bay (GTB), each having water-depths greater than 100 m. Data from both lakes were analyzed by use of a generalized additive models (GAM), which contained similar parametric and smooth terms. The GAM for Torch Lake explained 74.0, 81.5, and 63.8 percent of the variability of reflectances in blue, green, and red bands, respectively. The GAM for GTB explained a corresponding 56.1, 43.7, and 41.8 percent of the variability in reflectances, which is attributed to lower variability in GTB data without both deep and shallow water-depth intervals.

The seasonal components of reflectances for both Torch Lake and GTB were highest on March 1 and November 30 for all bands. All bands for GTB and the red band for Torch Lake decreased monotonically from March 1 to early September before increasing to November 30, showing a similar range of amplitudes. The seasonal component of the blue and green bands in Torch Lake, however, also had a minimum in June and a secondary peak in late August, which receded to a secondary minimum in late October before increasing at the end of the open-water season. The amplitude of the seasonal response varied with water-depth interval having larger amplitude variations with greater depth intervals, especially for the blue band, which also had the highest reflectances.

In this report, trend is interpreted from patterns in local levels estimated within the GAM models. For Torch Lake, the local levels for blue and green bands showed generally positive deviances (from zero) for the period from 1984 to 2010. After 2010, local levels rapidly attained negative deviances, which leveled off after 2021. Amplitudes of local levels were generally greater in the blue band than the green band, and greater in the shallower water-depth intervals than the deeper depths. The red band showed a generally linear decrease in magnitude throughout the period of record with little variability between water-depth intervals. Local levels derived from the GTB GAM showed similar non-monotonic, but generally decreasing, magnitudes.

The occurrence and growth of benthic algae would likely be most evident in shallow areas of the lake where the overlying water-column thickness is at a minimum. Prior to the late 1990s, surface reflection intensities in the green band, and to a lesser extent in the blue band, were less at shallower depths. Following the late 1990s to about 2010, a transition occurred in which the shallow water reflectance intensities exceeded those in deeper waters. This shift in the photosynthetically active green and blue bands may correspond to changes in algae populations.

Possible differences in measurement precision among satellites was investigated by comparing the probability densities of GAM residuals by satellite identifier using violin plots. No substantial differences in mean values or variabilities were apparent among satellites for the blue, green, and red bands used in this analysis. Also, time series of GAM residuals were inspected for possible trends. The GAM models included a factor variable for individual satellites, which were highly significant. Changes in defined band width intervals spanning the blue, green, and red visible light spectrum between the LT05 and LE07 satellites and the LC08 and LC09 satellites may have contributed to the significance of these variables. These minor changes in band width intervals may have been exacerbated by the relatively low reflectance characteristics of aquatic surfaces relative to the broader range of reflectances associated with land surfaces. Once these difference in levels were removed by the factor variables, however, there were no apparent bias attributable to individual satellites.

The common assumption of independent and identically distributed model residuals was investigated in the analysis. In particular, the assumption of spatial independence was of concern because Torch Lake was stratified into two basins and five water-depth intervals. Thus, each satellite image contributed 10 data points for each date of measurement. As atmospheric conditions varied with the date of measurement and likely affected reflectance in a similar way for each strata on that date, spatial correlation of errors were likely. Analysis indicated that correlations exceeding 0.90 were commonly associated with model errors at deeper water-depth intervals (50-100 ft, 100-200 ft, and >200 ft). These correlations would likely reduce the statistical significance of a model component, thereby increasing the magnitudes of some p-values reported in tables 8, 9, and 10. Thus, some caution should be used when interpreting the exact statistical significance of differences between relectances in deeper water-depth intervals. No appreciable temporal correlation errors were detected.

In general, the magnitudes, timings, and band-specific characteristics of seasonal variations and local levels of Torch Lake and GTB were dissimilar, discounting concerns about a common factor associated with flaws in the satellite imagery. More likely, the seasonal and temporal variations reflect physical, chemical, and biological processes in the lakes that are yet to be fully explained. It is hoped that information in this report provides a context to help improve the understanding of processes in Torch Lake.

References Cited

Allaire, J. J., and Christophe. Dervieux. 2024. *Quarto: R Interface to 'Quarto' Markdown Publishing System*. https://CRAN.R-project.org/package=quarto.

Amand, Ann St. 2020. "Identification of Freshwater Algae." Michigan Inland Lakes Convention; https://mediaspace.msu.edu/media/WorkshopA+Algal+Identification+9+18+2020/1_9dzq5xck.

Google. 2024a. "Google Earth Engine: A Planetary-Scale Platfrom for Earth Science Data & Analysis." https://earthengine.google.com/.

———. 2024b. "Google Earth Engine: Get Started with Earth Engine." https://developers.google.com/earth-engine/guides/getstarted.

Katsaros, K. B., McMurdie, L. A., R. J. Lind, and J. E. DeVault. 1985. "Albedo of a Water Surface, Spectral Variation, Effects of Atmospheric Transmittance, Sun Angle and Wind Speed." *Journal of Geophysical Research* 90 (C4): 7313–21. https://doi.org/https://doi.org/10.1016/j.solener.2019.02.040.

Katz, Ellie. 2023. "With Golden Brown Algae, Searching for Answers Leads to More Questions." https://www.interlochenpublicradio.org/ipr-news/2023-10-04/with-golden-brown-algae-searching-for-answers-leads-to-more-questions/; Interlochen Public Radio. 2023.

Levesque, V. A., and K. A. Oberg. 2012. "Computing Discharge Using the Index Velocity Method." Edited by U. S. Geological Survey. Techniques and Methods. Reston, VA. https://doi.org/10.3133/tm3A23.

Maciel, D. A., Pahlevan N., Barbosa C. C. F., de Moraes de Novo E. M. L., Paulino R. S., Martins V. S., Vermote E., and C. J. Crawford. 2023. "Validity of the Landsat Surface Reflectance Archive for Aquatic Science: Implications for Cloud-Based Analysis." *Limnology and Oceanography Letters* Vol. 8, issue 6. https://doi.org/10.1002/lol2.10344.

Michigan Department of Natural Resources. 2023. "Inland Lake Contours." https://gis-michigan.opendata.arcgis.com/datasets/Michigan::inland-lake-contours/about.

Moore, D. S., Notz W. I., and M. A. Flinger. 2011. *The Basic Practice of Statistics*. W.H. Freeman; Company.

NOAA National Geophysical Data Center. 1996. "Bathymetry of Lake Michigan, Ridges and Valleys in the Islands Area (area 6, subarea 7)." https://www.ngdc.noaa.gov/mgg/greatlakes/lakemich_cdrom/html/geomorph.htm. https://doi.org/10.7289/V5B85627.

Posit team. 2024. *RStudio: Integrated Development Environment for r*. Boston, MA: Posit Software, PBC. http://www.posit.co/.

R Core Team. 2024. *R: A Language and Environment for Statistical Computing*. Vienna, Austria: R Foundation for Statistical Computing. https://www.R-project.org/.

Rocchio, Laura E.P. 2023. "Researchers Caution Use of Landsat's Land-Specific Surface Reflectance Products for Long-Term Water Quality Studies." https://landsat.gsfc.nasa.gov/article/researchers-caution-use-of-landsats-land-specific-surface-reflectance-products-for-long-term-water-quality-studies/.

Tip of the Mitt Watershed Council. 1987a. "Comprehensive Water Quality Monitoring." https://watershedcouncil.org/projects/comprehensive-water-quality-monitoring/.

———. 1987b. "Volunteer Lake Monitoring." https://watershedcouncil.org/projects/volunteer-lake-monitoring/.

Torch Conservation Center. 2024. "Waterpedia: Golden Brown Algae - Torch Conservation Center." https://conservetorch.org/algae/.

U.S. Forest Service. 2024(?). "Tannins." https://www.fs.usda.gov/wildflowers/ethnobotany/tannins.shtml.

U.S. Geological Survey. 2020. "USGS National Hydrography Dataset Plus High Resolution (NHDPlus HR) for 4-Digit Hydrologic Unit - 0406 (Published 20200327): U.s. Geological Survey." https://www.sciencebase.gov/catalog/item/5e7ecbd5e4b01d50927719a5.

———. 2021. "Landsat Collection 1 Vs Collection 2 Summary | u.s. Geological Survey."

https://www.usgs.gov/media/files/landsat-collection-1-vs-collection-2-summary.

———. 2024a. "How Do i Use a Scale Factor with Landsat Level-2 Science Products? | u.s. Geological Survey." https://www.usgs.gov/faqs/how-do-i-use-a-scale-factor-landsat-level-2-science-products.

———. 2024b. "Landsat Collection 2 Quality Assessment Bands." https://www.usgs.gov/landsat-missions/landsat-collection-2-quality-assessment-bands.

———. 2024c. "Landsat Provisional Aquatic Reflectance." https://www.usgs.gov/landsat-missions/landsat-provisional-aquatic-reflectance.

———. 2024d. "Landsat Satellite Missions." https://www.usgs.gov/landsat-missions/landsat-satellite-missions.

Wood, S.N. 2006. *Generalized Additive Models: An Introduction with r*. 1st ed. Chapman; Hall/CRC.

Appendix 1. Example JavaScript used in Google Earth Engine to access imagery

```
// Example JavaScript to extract summary statistics from LE07 images during POR.
// Torch Lake polygon outline is based on NHD waterbody outline
// Bathymetry contours of 5-, 50-, 100-, 150-, 200-, and with >250-ft contours dropped
// ROI is based on the -30m buffer fron NHD waterbody boundary for Torch Lake

// Torch Lake bath polygons is based on NHD as 0 -30m buffer
// with minor adjustments to 5 and 50 contorus and with 250+ contours dropped
// ROI is based on the -30m buffer fron NHD waterbody boundary for Torch Lake


// The shoreline of Torch Lake is based on the USGS NHDPlus HR coverage for
// waterbodies. The `ROI` (region of interest) is defined as a variable (var)
// that is offset 30 m from the shoreline to exclude parts of the lake
// where reflectance may be effected by trees overhanging the lake, docks, or
// other fixed obstructions on the lake.
var ROI = ee.FeatureCollection("projects/ee-dholtschlag/assets/Torch_Lake_NHD_Buffer_30");

// The variable `torch_lake_bath_poly` is defined as a set of nested polygons in
// which the outermost polygon is the ROI and the inner polygons are bounded by the
// 5-, 50-, 100-, 150-, 200-, and >200-ft countours.
var torch_lake_bath_poly =
   ee.FeatureCollection("projects/ee-dholtschlag/assets/Torch_Lake_NHD_Polygon_Bath");

// Temporal limits for Landsat 7 data
var startYear = 1999;  // start year
var endYear   = 2021;  // end year


// Access the image collection  LANDSAT/LE07/C02/T1_L2 that includes Landsat
// LE07 data, collection 2, tier 1, level 2 data only. Spatial and temporal
// limits are applied to include seasonal periods from March 1 to November 30.
var filteredCollectionL7 = ee.ImageCollection('LANDSAT/LE07/C02/T1_L2')
    .filterBounds(ROI)
    .filter(ee.Filter.calendarRange(3, 11, 'month'))
    .filterDate(ee.Date.fromYMD(startYear, 3, 1), ee.Date.fromYMD(endYear, 11, 30))
    .map(function(image) { return image.set('satellite', 'Landsat 7'); });

// function defined for Masks for clouds, cloud shadow, and snow/ice are consistent for all satellites
function maskLandsat(image) {
  var sensor = image.get('SENSOR_ID');
  var cloudMask       = image.select('QA_PIXEL').bitwiseAnd(1 << 5).eq(0);
  var cloudShadowMask = image.select('QA_PIXEL').bitwiseAnd(1 << 3).eq(0);
  var snowIceMask     = image.select('QA_PIXEL').bitwiseAnd(1 << 4).eq(0);
  var combinedMask    = cloudMask.and(cloudShadowMask).and(snowIceMask);
  return image.updateMask(combinedMask)
}
```

```
// function defined for computing statistics for each polygon contour interval
function computeStats(image) {
    var selectedImage = image.select(['SR_B1', 'SR_B2', 'SR_B3']);
    var reduced = torch_lake_bath_poly.map(function(feature) {
        var statistics = selectedImage.reduceRegion({
            reducer: ee.Reducer.mean().combine({
                reducer2: ee.Reducer.median(),
                sharedInputs: true
            }).combine({
                reducer2: ee.Reducer.percentile([0, 2, 5, 10, 25, 50, 75, 90, 95, 98, 100]),
                sharedInputs: true
            }).combine({
                reducer2: ee.Reducer.count(),
                sharedInputs: true
            }).combine({
                reducer2: ee.Reducer.stdDev(),
                sharedInputs: true
            }),
            geometry: feature.geometry(),
            scale: 30,
            maxPixels: 1e9
        });
        return feature.set(statistics)
                      .set('timestamp',          selectedImage.date().format('YYYY-MM-dd HH:mm'))
                      .set('satellite',          selectedImage.get('satellite'))
                      .set('WRS_ROW',            selectedImage.get('WRS_ROW'))
                      .set('WRS_PATH',           selectedImage.get('WRS_PATH'))
                      .set('CLOUD_COVER',        selectedImage.get('CLOUD_COVER'))
                      .set('IMAGE_QUALITY_OLI',  selectedImage.get('IMAGE_QUALITY_OLI'))
                      .set('LANDSAT_SCENE_ID',   selectedImage.get('LANDSAT_SCENE_ID'))
                      .set('LANDSAT_CENTER_TIME',selectedImage.get('LANDSAT_CENTER_TIME'))
                      .set('SUN_AZIMUTH',        selectedImage.get('SUN_AZIMUTH'))
                      .set('SUN_ELEVATION',      selectedImage.get('SUN_ELEVATION'))
    });
    return reduced;
}

// Apply the maskLandsat function to the image collection within the ROI
var maskedCollectionL7 = filteredCollectionL7.map(maskLandsat);

// Apply the computeStats function to the masked collection
var statsCollection    = maskedCollectionL7.map( computeStats );
print("statsCollection", statsCollection);

// function defined to determine the number of properties a feature has and
// to drop data for images having fewer than 50 properties, which implies
// that there were not enough valid pixels to compute statistics on image.
function filterFeaturesWithMoreProperties(feature) {
  // Get the properties of the feature
  var properties = feature.toDictionary();
  // Check the number of properties
```

```
  var numProperties = ee.Dictionary(properties).size();
  // Return true for features with more than 7 properties
  return numProperties.gt(50);
}

// Add a property 'numProperties' to each feature which tells the number of
// properties that feature has.
var addPropertyCount = function(feature) {
  var propertyList = feature.propertyNames();
  var numProperties = ee.Number(propertyList.size());
  return feature.set('numProperties', numProperties);
};

// Apply addPropertyCount function to statsCollection
var standardizedFeatures = statsCollection.filter(ee.Filter.neq('addPropertyCount', 7));
var featuresWithPropertyCount = standardizedFeatures.map(addPropertyCount);

// Now, filter out features based on the number of properties.
var desiredFeatures = featuresWithPropertyCount.filter(ee.Filter.neq('numProperties', 49));

// Apply function `flatten` to create column-oriented dataset
var flatStats = statsCollection.flatten();
print('flatStats', flatStats);

// Add a property to each feature that represents the count of properties
function addPropertyCount(feature) {
  var count = ee.Number(ee.List(feature.propertyNames()).length());
  return feature.set('numProperties', count);
}

var withPropertyCounts = flatStats.map(addPropertyCount);
print('withPropertyCounts', withPropertyCounts);

// Now, filter based on the added property count
var filteredFeatures = withPropertyCounts.filterMetadata('numProperties', 'greater_than', 50);

// Export data
Export.table.toDrive({
    collection: filteredFeatures,
    description: 'TL_LE07C2T1L2_1999_2021_Mask234_TL_NHD_30mBuffer',
    folder: 'Torch',
    fileNamePrefix: 'LE07C2T1L2_1999_2021_Mask345_TL_NHD_30mBuffer',
    fileFormat: 'CSV'
});
```